# Crystal-Packing Trends for a Series of 6,9,12,15,18-Pentaaryl-1-hydro[60]fullerenes

**Robert D. Kennedy, Merissa Halim, Saeed I. Khan, Benjamin J. Schwartz, Sarah H. Tolbert, and Yves Rubin*[a]**

**Abstract:** The relationship between the size of the substituents of aryl groups in a series of fifteen 6,9,12,15,18-pentaaryl-1-hydro[60]fullerenes and the solid-state structures and packing motifs of these compounds has been analyzed. Pentaarylfullerenes have a characteristic "badminton shuttlecock" shape that causes several derivatives to crystallize into columnar stacks. However, many pentaarylfullerenes form non-stacked structures with, for example, dimeric, layered, diamondoid, or feather-in-cavity relationships between molecules. Computational modeling gave a qualitative estimate of the best shape match between the ball and socket surfaces of each pentaarylfullerene. The best match was for pentaarylfullerenes with large, spherically shaped *para*-substituents on the aryl groups. The series of pentaarylfullerenes was characterized by single-crystal X-ray diffraction. A total of 34 crystal structures were obtained as various solvates and were categorized by their packing motifs.

**Keywords:** fullerenes · host–guest interactions · self-assembly · solid-state structures · stacking interactions

## Introduction

The electronic properties of the fullerenes and their derivatives have been crucial to the development of bulk-heterojunction organic photovoltaic devices (BHJ OPVDs).[1,2,3,4,5] Until recently, improvements in the efficiency of BHJ OPVDs were obtained primarily through optimization of device fabrication and the use of low-bandgap electron-donating conjugated polymers to expand light absorption across the visible range.[1] Lately, however, modification of the electron-accepting fullerene component of OPVDs has contributed significantly to advances in this area through better matching of the frontier orbital energy levels between donor polymer and fullerene acceptor.

It is worth noting that [6,6]-phenyl-$C_{61}$-butyric acid methyl ester ([60]PCBM) is still one of the best electron acceptors in OPVDs, despite the fact that it was the first derivative of a fullerene to be used in a BHJ OPVD. This is mainly because [60]PCBM exerts an optimal influence on the morphology and phase separation of regioregular poly(3-hexylthiophene) (P3HT) and other donor polymers.[6] More recently, several fullerene-derived acceptors have led to OPVDs with efficiencies surpassing those based on

[60]PCBM.[2b,d,g,j] For continued improvement of OPVD efficiency, there is a need for novel fullerene derivatives in addition to better polymers, in part to further tune the electronic parameters of the electron-acceptor component by better complementing that of the polymer donor and also to further optimize the active-layer morphology of the BHJs. Furthermore, to enhance light absorption of the acceptor across the visible spectrum, novel fullerene derivatives, such as the $C_{70}$ homologue ([70]PCBM) of [60]PCBM, have been increasingly used to obtain state-of-the-art devices.[2b,7] Further improvements of all these aspects should ultimately bring superior OPVDs to the market.

Altering the nature of the addends and the addition pattern on the fullerene surface gives exquisite control over the energy levels of the fullerene frontier molecular orbitals. Substituent manipulation also helps to fine-tune intermolecular interactions within and between the donor and acceptor components in the active layer of a BHJ device. However, the majority of fullerene derivatives have been decidedly PCBM-like, possessing a fused cyclopropane ring across a 6,6-bond of $C_{60}$ with an appended aromatic or heteroaromatic ring and an alkyl substituent that often incorporates an ester group.[2c,e,f,i,3] This mimicking of the PCBM architecture can present advantages in that the electronic structure of the fullerene core is largely preserved within a similar series, which allows an assessment of the substituent influence on solubility and nanoscale morphology of the BHJ, and its effect on device efficiency. However, for further advancement in this area, innovative approaches to developing novel fullerene acceptors are necessary and are starting to emerge.[2d,g,j–m,3,8,9]

Our group has examined 6,9,12,15,18-pentaaryl-1-hydro[60]fullerenes (**1**, Scheme 1) as novel electron acceptors

[a] Dr. R. D. Kennedy, M. Halim, Dr. S. I. Khan, Prof. B. J. Schwartz,
Prof. S. H. Tolbert, Prof. Y. Rubin
Department of Chemistry and Biochemistry
University of California, Los Angeles
607 Charles E. Young Drive East
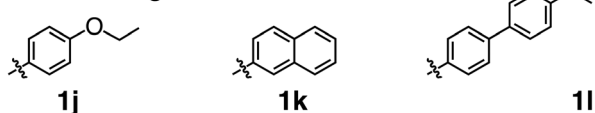Los Angeles, CA 90095 (USA)
E-mail: rubin@chem.ucla.edu

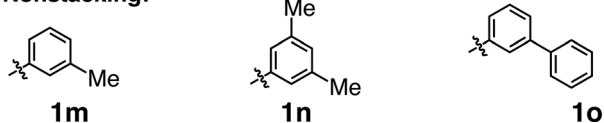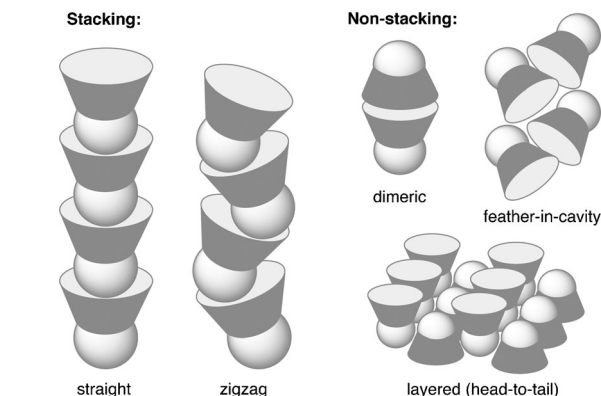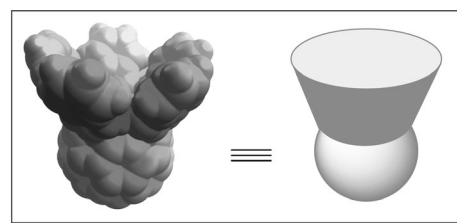Supporting information for this article is available on the WWW under http://dx.doi.org/10.1002/chem.201103400.
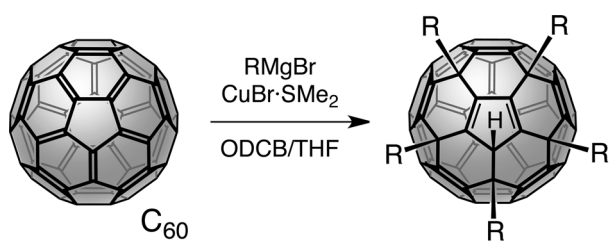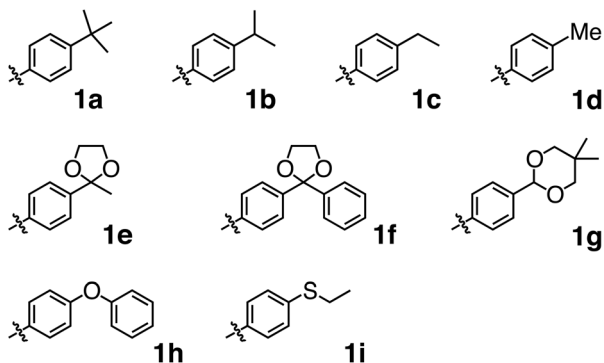
Scheme 1. General synthetic scheme for the 6,9,12,15,18-pentaaryl-1-hydro[60]fullerenes **1a–o** and structures of the R addends. Each derivative is classified by a particular crystal-packing motif. However, several derivatives crystallize within several motifs depending on the included solvent, as reported in Tables 1 and 2.



Scheme 2. Representations of straight- and zigzag-stacked motifs, as well as representative non-stacking motifs, such as dimeric, feather-in-cavity, and layered, found in the crystal structures of the 6,9,12,15,18-pentaaryl-1-hydro[60]fullerenes **1a–o**.

in BHJ OPVDs, together with P3HT as the light-absorbing electron-donor, mainly because their intriguing molecular shape leads them to form one-dimensional stacks.[8,9] Pentaarylfullerene derivatives form columnar stacks in the solid state and even in solution by nestling the ball-shaped fullerene subunit of **1** into the cavity formed by the five aryl addends of an adjacent molecule, which gives straight or zigzag stacks (Scheme 2).[8,10] With nonpolar groups, this process is driven by a range of van der Waals interactions. The question of whether stacking interactions could favor higher electron mobility values within the fullerene phase of BHJ photovoltaic devices was initially examined by our group.[8] Nakamura subsequently reported BHJ OPVDs incorporating a similar series of compounds.[11]

In our preliminary study, we observed that *m*-tolyl fullerene derivative **1m** (Scheme 1), which forms an *ortho*-dichlorobenzene (ODCB) solvate with a dense two-dimensional network of C⋯C close contacts between the fullerene π surfaces in the solid state (non-stacked, layered head-to-

tail motif of Scheme 2),[8] performs much less efficiently in BHJ OPVDs with P3HT as the donor polymer than 4-*tert*-butylphenyl derivative **1a**, which has a solvent-independent straight-stacking motif (Scheme 2) with no C⋯C close contacts (shortest C⋯C distance of ca. 4.3 Å). Assuming a model in which electron transfer between fullerene subunits is promoted by close contact of the π systems, this result was counterintuitive; we suggested that the self-assembly of pentaarylfullerene molecules critically influences polymer crystallinity and the resulting nanoscale morphology of the films, and that molecular-scale factors, such as the proximity of molecules within a single crystal of the pentaarylfullerene or its solvate, are not necessarily direct determinants of the BHJ device efficiency. However, our observation contrasted with that reported by Hummelen,[12] who investigated the solvent-dependent crystal packing of [60]PCBM and found that a three-dimensional network of short C⋯C contacts between fullerene bodies is produced when crystals are grown from PhCl, whereas a two-dimensional network is produced when ODCB is used. The two crystallization modes of [60]PCBM correlated well with the observation that a BHJ OPVD containing [60]PCBM and poly[2-methoxy-5-(3′,7′-dimethyloctyloxy)-1,4-phenylene vinylene] (MDMO-PPV) performs more efficiently when fabricated by using PhCl rather than ODCB. Hummelen attributed the increased efficiency in part to facilitated electron transport through the denser three-dimensional network of short π–π contacts between fullerene moieties within [60]PCBM crystallites. However, the influence of the solvent on thin-film morphology was also viewed as a possible important factor in the enhancement of device efficiency.

The parameters affecting molecular interactions between pentaarylfullerenes in the solid state needed to be investigated in more depth.[8,9] The present study scrutinizes the crystal-packing trends for a series of chemically and structurally related pentaarylfullerenes (1a–o), focusing on the robustness of stacking motifs, that is, the propensity of each pentaarylfullerene derivative to form a solvent-independent stacking motif (universal stacker). In addition, factors such as the density of short C···C contacts (below the sum of the van der Waals radii) between the π systems of two fullerene moieties and the dimensionality of the close-contact networks they constitute have been analyzed.

## Results and Discussion

**Molecule and crystal design**: The principle behind this study is that molecular self-assembly of the fullerene acceptor component could lead to favorable phase separation within the active layer of a BHJ OPVD by preventing large crystallite formation.[8,9] Reinforcing long-range molecular order within the fullerene acceptor phase of OPVDs could also be a mechanism to achieve higher electron mobility.[13]

Accordingly, fullerene derivatives with a strong stacking tendency should help demonstrate this concept. The straight-stacked packing motif was already known from the crystal structure of the 4-biphenyl derivative (1, R = 4-PhC_6H_4), and the stacking concept was subsequently applied to several pentaarylfullerenes[10,11] and fullerene pentaadducts with an (aryldimethylsilyl)methyl group (1, R = CH_2SiMe_2Ar).[10d,16] Thus, the ease with which these molecules can be synthesized makes them especially attractive for the exploration of self-assembly principles and their possible effect on the nanoscale architecture and device performance of BHJ OPVDs.[8,9,10,11,17]

For the purpose of this work,[8,9] it was important to determine to what extent the shape of the aryl addends governs the stacking propensity of molecules of 6,9,12,15,18-pentaaryl-1-hydro[60]fullerene (1) in crystalline solids.[14] The addend groups ("feathers") on 6,9,12,15,18-pentaaryl-1-hydro[60]fullerenes (1) project radially from the quasi five-fold axis of these molecules, creating a socket that can accommodate a fullerene ball of complementary shape (Scheme 2, Figures 1 and 2). To study the influence of addend shape on stacking, the sizes and shapes of the alkyl substituents at the 3- or 4-positions of the five aryl groups of 1a–o were varied. Except for the ether, thioether or ketal functions of 1e–j, the other members of the series have nonpolar alkyl groups that maintain a similar polarity between molecules. Strong directional interactions, such as dipole–dipole or hydrogen bonding, were avoided because they can be detrimental to thin film morphology.[18]

Interestingly, the groups of Sokolov, as well as Matsuo and Nakamura, have reported the crystal structure of 6,9,12,15,18-pentamethyl-1-hydro-[60]fullerene (1, R = CH_3) as an example of one of the smallest stacking fullerenes (Figure 1a).[19] Sokolov suggested that the formation of col-
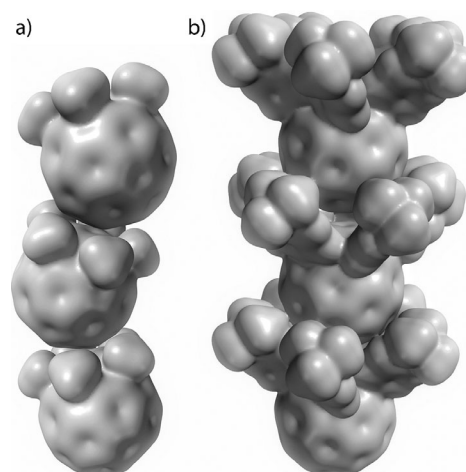


Figure 1. Representations of the electron-density envelopes (0.005 e au$^{-3}$) for 6,9,12,15,18-pentamethyl-1-hydro[60]fullerene (1, R = CH_3) and 6,9,12,15,18-pentakis(4-tert-butylphenyl)-1-hydro[60]fullerene 1a, and the two types of stacks formed by these shuttlecock molecules: a) zigzag and b) straight stacking. Electron density envelopes were generated from a PM3 single-point energy calculation on crystal-structure coordinates.[8,14,15,19a]

umnar stacks is general and independent of the nature of the addend.[20] However, we have found that a number of pentaarylfullerenes form nonstacked motifs (Scheme 1, Table 2), which indicates that stacking is far from general in these compounds.

Although current computational methods are starting to give reliable predictions for the crystal structures of organic molecules, they are still limited to small systems,[21] and pentaarylfullerenes 1a–o are beyond current computational capabilities using these methods. Thus, the substituents of the aryl addends in pentaarylfullerenes 1a–o were varied by examining qualitative computer models (Figure 2).[14,15] The socket depth increases dramatically depending on the size of the substituent on the phenyl group and the relative orientation of each aryl moiety. Bulkier phenyl substituents, especially those with a spheroidal or cylindrical shape, such as tert-butyl (1a), 1-[2.2.2]bicyclooctyl, or 1-adamantyl, are particularly effective at shaping the socket (Figure 2). Thus, the difference in socket depths between the pentaphenyl (1, R = Ph, Figure 2b), the 4-tert-butylphenyl (1a, Figure 2d), and the 4-(1-adamantyl)phenyl systems (1, R = 1-adamantyl, Figure 2g) is quite dramatic. Accordingly, phenyl groups with relatively large and spheroidal substituents at the 4-position are the best suited to promote stacking, as determined experimentally from their crystal structures (vide infra), whereas small addends (e.g., 1, R = CH_3 or Ph, Figure 2a,b) give sockets with a cavity that can be too shallow for efficient stacking.[19,20]

As described in our photovoltaic device studies,[8,9] 4-tert-butylphenyl system 1a currently offers the best compromise between aryl-substituent size, stacking ability, and device performance. Compound 1a is a "universally stacking" pentaarylfullerene that is moderately soluble in ODCB
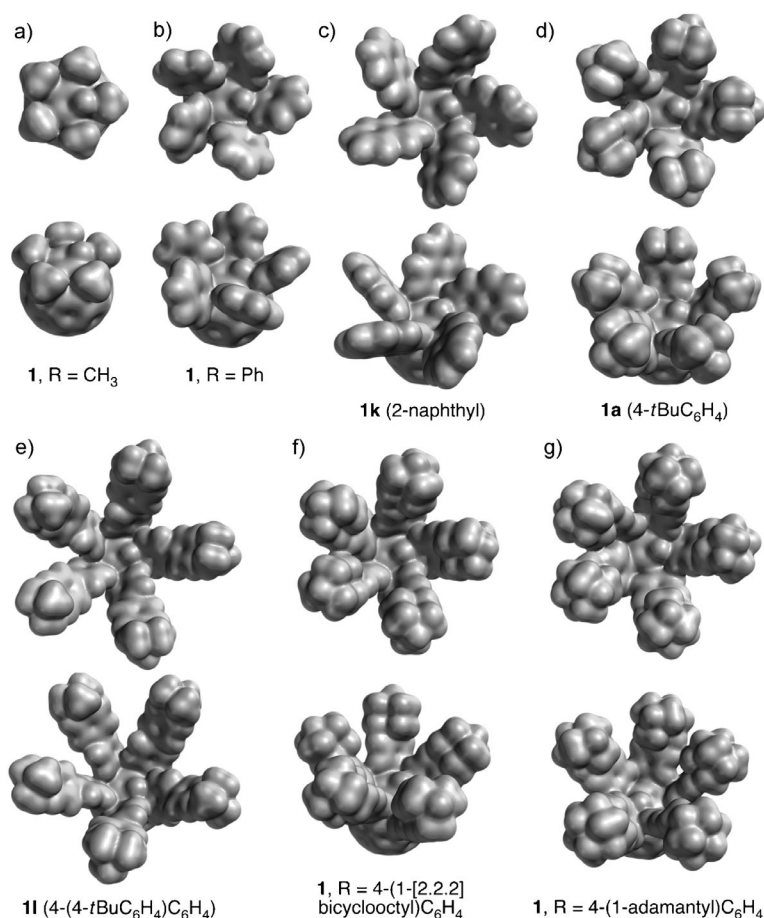
Figure 2. Electron-density envelopes (0.005 e au$^{-3}$) for a series of pentaarylfullerenes, showing the influence of aryl substituents on shape and bowl depth, calculated on PM3-optimized structures.[14] In each pairwise representation, the top view looks down the quasi five-fold axis of the molecule, whereas the bottom view is rendered side-on to help visualize bowl depth.

($\leq$10 mg mL$^{-1}$), which makes it well suited for spin-casting while keeping the substituent size to a minimum.

**Crystal-packing parameters**: For most members of the series of 6,9,12,15,18-pentaaryl-1-hydro[60]fullerenes (**1a–o**) with substitutions at the 3- or 4-positions of the phenylene moiety, crystals were grown from multiple solvent systems and evaluated by single-crystal X-ray diffraction (Tables 1, 2, and 3–5.[14,22] The extended solid-state structures of pentaarylfullerenes **1a–o** may be split into two general categories: stacking, as described above, and non-stacking, in which a stacking motif is not observed (Scheme 1, Figures 1 and 3, Tables 1–5). Each category is subdivided into more specific types of intermolecular interactions, such as straight and zigzag for the stacking motifs, and dimeric, diamondoid, layered, feather-incavity, or isolated for the nonstacking motifs (Scheme 2, Tables 1 and 2).

The following packing parameters are defined here to compare the different stacking modes observed in the crystal structures of compounds **1a–**

Table 1. Structural parameters for straight and zigzag-stacked pentaarylfullerenes (**1a–i**).

| | 1a[22] | 1a | 1b | 1b | 1c | 1d | 1e | 1f | 1f | 1g | 1g | 1g | 1h | 1i |
|---|---|---|---|---|---|---|---|---|---|---|---|---|---|---|
| R[a] | tBu | tBu | iPr | iPr | Et | Me | – | – | – | – | – | – | OPh | SEt |
| included solvent[24] | (n-C$_5$H$_{12}$)$_3$ | (PhCl)$_3$ | (PhCl)$_3$ | (1-ClNp)$_2$ | (CS$_2$)$_{0.5}$ | (PhMe)$_3$ | (PhMe)$_3$ | (PhCl)$_3$ | (CHCl$_3$)$_{2.5}$-(Et$_2$O)$_{0.5}$ | (PhOMe)$_2$ | (1-ClNp)$_2$ | (CS$_2$)$_3$ | ODCB | – |
| stacking motif | straight | straight | straight | zigzag | zigzag | zigzag | straight | straight | straight | zigzag | zigzag | straight | straight | zigzag |
| $S_D$ [Å] | 10.8 | 10.9 | 10.9 | 10.8 | 10.7 10.8 | 10.9 | 11.1 | 10.9 | 11.0 | 10.8 | 10.8 | 11.4 | 10.8 | 10.9 |
| $\Theta$ [°] | 177.8 | 179.4 | 172.9 | 126.4 | 136.5 | 115.9 | 167.9 | 171.6 | 172.6 | 133.5 | 139.6 | 180.0 | 174.1 | 132.9 |
| $I_D(ap_i)$ [Å] | 14.9 | 14.9 | 15.2 14.8 | 12.2 12.6 | 10.1 10.8 | 9.9 13.1 | 14.6 15.7 | 13.8 17.4 | 14.9 20.1 22.4 | 10.2 17.1 | 17.0 19.2 | 13.7 15.3 | 13.9 | 10.1 10.2 |
| $I_D(p_i)$ [Å] | 17.1 22.7 | 16.9 22.9 | 16.0 22.6 | 17.6 21.1 | 10.1 | 15.2 20.9 | 16.8 23.1 | 20.8 23.3 | 16.3 | 19.0 24.6 | 16.2 32.0 | 16.2 24.1 | 17.5 18.5 20.5 | 15.7 18.9 |
| $\rho_S \times 10^{-3}$ [Å$^{-2}$] | 5.1 | 5.4 | 5.5 | 4.8 | 6.8 | 5.4 | 5.1 | 4.1 | 4.5 | 4.1 | 3.9 | 5.1 | 5.6 | 6.5 |
| $\rho_F \times 10^{-4}$ [Å$^{-3}$] | 4.8 | 4.7 | 5.1 | 5.0 | 6.8 | 5.8 | 4.7 | 3.8 | 4.1 | 4.1 | 3.9 | 4.5 | 5.2 | 6.5 |

[a] Refers to a substituent at the 4-position of a phenyl group where indicated, otherwise refer to structures in Scheme 1.

Table 2. Structural parameters for dimeric and non-stacking pentaarylfullerenes **1b**, **1d**, and **1j**–**o**.[22]

| | Packing motif | Network order | $\rho_F \times 10^{-4}$ [Å$^{-3}$] | Av. no. of close contacts[a] |
|---|---|---|---|---|
| **1b**·CS$_2$ | feather-in-cavity | 1D | 5.95 | 2 |
| **1d**·(1-ClNp)(MeOH)$_{0.5}$ | dimer | 2D | 6.24 | 3 |
| **1j**·(CS$_2$)$_2$ | dimer | 2D | 6.13 | 3.5 |
| **1j**·PhMe | dimer | 3D | 6.08 | 4 |
| **1k**·(ODCB)$_{1.5}$ | dimer | 2D | 5.76 | 3 |
| **1k**·(CS$_2$)$_5$ | dimer | 1D | 5.01 | 2 |
| **1k**·(CH$_2$I$_2$)$_n$ | dimer | 1D | 4.70 | 2 |
| **1l**·($c$-C$_6$H$_{12}$)$_4$ | dimer | 0D | 3.42 | 1 |
| **1m**·CHCl$_3$ | diamondoid | 3D | 7.02 | 4 |
| **1m**·CS$_2$ | diamondoid | 3D | 7.01 | 4 |
| **1m**·PhMe | layered | 2D | 6.78 | 5 |
| **1m**·ODCB | layered | 2D | 6.72 | 5 |
| **1m**·(PhCl)$_2$ | layered | 2D | 6.27 | 3 |
| **1n**·($c$-C$_6$H$_{12}$)$_4$ | isolated | 0D | 4.84 | 1 |
| **1n**·(PhI)$_{0.5}$($n$-C$_5$H$_{12}$)$_{0.5}$ | feather-in-cavity | 2D | 6.25 | 3 |
| **1n**·(2-BrC$_4$H$_3$S) | feather-in-cavity | 2D | 6.30 | 3 |
| **1o**·(CS$_2$)$_{0.5}$($n$-C$_5$H$_{12}$)$_{0.5}$ | layered | 2D | 5.11 | 3 |

[a] Close contacts are defined as C$_{60}$ centroid-to-centroid distances of $\leq 10.5$ Å.

**i** (Figure 4). Within each stack, the intrastack angle $\Theta$ [°] and separation $S_D$ [Å] define the fundamental relationships between each molecule and its neighbors. At the next level of packing complexity, each stack is separated from neighboring stacks in a parallel or antiparallel fashion, with a corresponding range of interstack distances $I_D$ [Å]. These distances were calculated between centroids[23] of the nearest fullerene balls in antiparallel columns, defined as $I_D(ap_i)$ ([Å], $i = a, b, c$), or in parallel columns, defined as $I_D(p_i)$ ([Å], $i = a, b, c$). The exact number of interstack separation distances ($i = a, b, c$) is related to the space group of each crystal structure and is reported in Table 1. This simple nomenclature is sufficient to discuss all stacking systems based on pentaarylfullerenes **1a–i**, although it does not account for the specific orientation of each pentaarylfullerene in relation to another molecule within or across stacks, or the relative orientations of individual aryl groups within each pentaarylfullerene, which are discussed in more depth in the Supporting Information. In addition, stack density $\rho_S$ ($\times 10^{-3}$ Å$^{-2}$) and fullerene density $\rho_F$ ($\times 10^{-4}$ Å$^{-3}$) parameters were calculated (Tables 1 and 2) to discuss the density of fullerene–fullerene $\pi$–$\pi$ contacts in crystals. The fullerene density $\rho_F$ was obtained by dividing the number of fullerenes contained in the unit cell by the volume of the unit cell, whereas the stack density $\rho_S$ was obtained by dividing the number of stacks by the area perpendicular to the stack axes.

### Crystal-packing trends

*Straight-stacked systems*: The formation of a straight-stacked packing motif is strongly dependent on the presence of aryl

Table 3. Crystallographic data for pentaarylfullerenes **1a–d** crystallized from several solvents.[25]

| | **1a** | **1a** | **1b** | **1b** | **1c** | **1d** | **1d** |
|---|---|---|---|---|---|---|---|
| crystal formula | **1a**·(PhCl)$_3$ | **1a** [squeeze] | **1b**·CS$_2$ | **1b**·($n$-C$_6$H$_{14}$)$_{0.5}$ (ODCB)$_{0.5}$ | **1c**·(CS$_2$)$_{0.5}$ | **1d**·(PhMe)$_{2.7}$ | **1d** [squeeze] |
| chemical formula | C$_{128}$H$_{80}$Cl$_3$ | C$_{110}$H$_{65}$ | C$_{106}$H$_{51}$S$_2$ | C$_{111}$H$_{64}$Cl | C$_{201}$H$_{92}$S$_2$ | C$_{113.9}$H$_{56.6}$ | C$_{95}$H$_{35}$ |
| $M_r$ [g mol$^{-1}$] | 1724.27 | 1386.62 | 1388.59 | 1433.07 | 2570.87 | 1424.99 | 1176.23 |
| crystal system[a] | orthorhombic | orthorhombic | orthorhombic | monoclinic | triclinic | monoclinic | triclinic |
| space group | $Pna2_1$ | $Pnma$ | $Pnma$ | $P2_1/c$ | $P\bar{1}$ | $P2_1/c$ | $P\bar{1}$ |
| $a$ [Å] | 21.910(2) | 21.7729(14) | 10.6333(8) | 17.469(7) | 15.121(2) | 15.245(3) | 14.3736(18) |
| $b$ [Å] | 16.8482(15) | 22.7282(14) | 19.3850(14) | 19.861(8) | 18.359(3) | 24.578(5) | 16.124(2) |
| $c$ [Å] | 22.946(2) | 17.0383(11) | 32.617(2) | 20.046(8) | 23.457(5) | 18.528(4) | 16.200(4) |
| $\alpha$ [°] | 90 | 90 | 90 | 90 | 104.584(2) | 90 | 109.678(2) |
| $\beta$ [°] | 90 | 90 | 90 | 98.853(4) | 97.222(3) | 98.741(2) | 97.706(2) |
| $\gamma$ [°] | 90 | 90 | 90 | 90 | 107.505(2) | 90 | 109.4330(10) |
| $V$ [Å$^3$] | 8470.6(13) | 8431.6(9) | 6723.1(9) | 6872(5) | 5865.2(18) | 6862(2) | 3203.2(10) |
| $Z$ | 4 | 4 | 4 | 4 | 2 | 4 | 2 |
| $\rho_{calcd}$ [g cm$^{-3}$] | 1.352 | 1.092 | 1.372 | 1.385 | 1.456 | 1.379 | 1.220 |
| $\mu$ [cm$^{-1}$] | 0.168 | 0.062 | 0.138 | 0.116 | 0.117 | 0.078 | 0.070 |
| $F(000)$ | 3596 | 2900 | 2876 | 2988 | 2660 | 2960 | 1210 |
| $2\theta_{min}, 2\theta_{max}$ [°] | 7.60 | 7.40 | 7.62 | 7.36 | 7.86 | 7.76 | 7.60 |
| | 52.82 | 52.58 | 56.50 | 58.66 | 57.92 | 49.42 | 56.38 |
| reflns. collected | 63 692 | 8737 | 57 878 | 91 891 | 94 902 | 73 650 | 28 490 |
| no. unique reflns. | 17 209 | 8737 | 8518 | 18 673 | 30 457 | 11 568 | 15 208 |
| $R_{int}$ | 0.098 | 0.0740 | 0.0325 | 0.0492 | 0.0664 | 0.098 | 0.0663 |
| obsd. reflns. [$I > 2\sigma(I)$] | 8934 | 5118 | 6823 | 12 052 | 16 003 | 5321 | 5803 |
| parameters/restraints | 1231/97 | 602/50 | 523/3 | 1026/82 | 1905/71 | 1038/73 | 861/0 |
| $R_1, wR_2$ | 0.0812 | 0.0922 | 0.0787 | 0.0983 | 0.0678 | 0.0829 | 0.0762 |
| (obsd. data) | 0.1908 | 0.2595 | 0.2227 | 0.2719 | 0.1571 | 0.1984 | 0.2036 |
| $R_1, wR_2$ | 0.1670 | 0.1377 | 0.0944 | 0.1407 | 0.1470 | 0.1890 | 0.1658 |
| (all data) | 0.2395 | 0.2872 | 0.2393 | 0.3096 | 0.1910 | 0.2523 | 0.2394 |
| GOF on $F_o^2$ | 0.985 | 1.055 | 1.098 | 1.074 | 1.049 | 1.073 | 0.826 |
| $\Delta$ [e Å$^{-3}$] | 0.071 | 0.341 | 0.930 | 0.849 | 1.003 | 0.442 | 0.388 |
| | −0.392 | −0.288 | −1.108 | −0.897 | −0.957 | −0.392 | −0.335 |

[a] All data were collected at 100 K.

Table 4. Crystallographic data for pentaarylfullerenes **1e–i** crystallized from several solvents.[25]

| | 1e | 1f | 1f | 1g | 1g | 1h | 1i |
|---|---|---|---|---|---|---|---|
| crystal formula | **1e**·(PhMe)$_3$ | **1f**·(CHCl$_3$)$_{2.5}$ (Et$_2$O)$_{0.5}$ | **1f**·(PhCl)$_{1.95}$ | **1g**·(CS$_2$)$_3$ | **1g**·(1-NpCl)$_2$ | **1h**·(ODCB) | **1i** |
| chemical formula | C$_{131}$H$_{79}$O$_{10}$ | C$_{139.5}$H$_{73.5}$Cl$_{7.5}$O$_{10.5}$ | C$_{146.70}$H$_{74.75}$Cl$_{1.95}$O$_{10}$ | C$_{123}$H$_{76}$O$_{10}$S$_6$ | C$_{140}$H$_{90}$Cl$_2$O$_{10}$ | C$_{126}$H$_{49}$Cl$_2$O$_5$ | C$_{100}$H$_{46}$S$_5$ |
| $M_r$ [g mol$^{-1}$] | 1812.94 | 2183.36 | 2066.34 | 1906.20 | 2003.02 | 1713.55 | 1407.67 |
| crystal system[a] | monoclinic | monoclinic | monoclinic | monoclinic | monoclinic | tetragonal | monoclinic |
| space group | $P2_1/n$ | $P2_1/n$ | $P2_1/c$ | $P2_1/m$ | $P2_1/n$ | $P\bar{4}2_1c$ | $P2_1/c$ |
| $a$ [Å] | 16.826(8) | 17.4498(12) | 24.922(2) | 11.3956(11) | 16.2040(4) | 26.8069(9) | 15.7227(14) |
| $b$ [Å] | 22.077(11) | 27.9548(19) | 20.7951(19) | 24.122(2) | 20.2280(5) | 26.8069(9) | 20.3556(18) |
| $c$ [Å] | 23.116(12) | 21.5941(15) | 21.639(2) | 16.2288(16) | 31.9909(8) | 21.6204(14) | 19.9096(18) |
| $\alpha$ [°] | 90 | 90 | 90 | 90 | 90 | 90 | 90 |
| $\beta$ [°] | 90.558(6) | 112.2870(10) | 111.1330(10) | 93.4720(10) | 98.510(2) | 90 | 104.5930(10) |
| $\gamma$ [°] | 90 | 90 | 90 | 90 | 90 | 90 | 90 |
| $V$ [Å$^3$] | 8587(7) | 9746.8(12) | 10460.5(16) | 4452.9(7) | 10370.4(4) | 15536.6(12) | 6166.4(10) |
| $Z$ | 4 | 4 | 4 | 2 | 4 | 8 | 4 |
| $\rho_{calcd}$ [g cm$^{-3}$] | 1.402 | 1.488 | 1.312 | 1.422 | 1.283 | 1.465 | 1.516 |
| $\mu$ [cm$^{-1}$] | 0.088 | 0.290 | 0.129 | 0.224 | 1.086 | 0.154 | 0.249 |
| $F(000)$ | 3780 | 4488 | 4272 | 1980 | 4176 | 7032 | 2904 |
| $2\theta_{min}, 2\theta_{max}$ [°] | 7.38 | 7.60 | 7.48 | 7.64 | 5.18 | 7.78 | 7.62 |
| | 50.70 | 56.72 | 52.88 | 58.14 | 68.31 | 56.58 | 58.20 |
| reflns. collected | 60614 | 87265 | 81338 | 42211 | 70624 | 137223 | 57715 |
| no. unique reflns. | 15596 | 24140 | 21428 | 12058 | 18048 | 19154 | 16446 |
| $R_{int}$ | 0.0949 | 0.0713 | 0.0666 | 0.0446 | 0.0484 | 0.0700 | 0.0621 |
| obsd. reflns. [$I > 2\sigma(I)$] | 7687 | 12789 | 12340 | 8134 | 13649 | 14468 | 9655 |
| parameters/restraints | 1296/2028 | 1451/8 | 1442/16 | 657/0 | 1446/67 | 1127/0 | 948/131 |
| $R_1$, $wR_2$ | 0.0829 | 0.0733 | 0.0762 | 0.0882 | 0.0925 | 0.1044 | 0.1468 |
| (obsd. data) | 0.2030 | 0.1861 | 0.2139 | 0.1587 | 0.2402 | 0.2188 | 0.2615 |
| $R_1$, $wR_2$ | 0.1735 | 0.1462 | 0.1256 | 0.0566 | 0.0776 | 0.0762 | 0.0901 |
| (all data) | 0.2633 | 0.2265 | 0.2377 | 0.1410 | 0.2273 | 0.1978 | 0.2249 |
| GOF on $F_o^2$ | 1.018 | 1.046 | 1.066 | 1.049 | 1.105 | 1.101 | 1.112 |
| $\Delta$ [e Å$^{-3}$] | 0.598 | 0.979 | 0.859 | 0.432 | 0.873 | 0.979 | 0.969 |
| | −0.410 | −0.846 | −0.651 | −0.540 | −1.005 | −0.730 | −1.015 |

[a] All data were collected at 100 K.

Table 5. Crystallographic data for pentaarylfullerenes **1j–o** crystallized from several solvents.[25]

| | 1j | 1k | 1k | 1n | 1n | 1o |
|---|---|---|---|---|---|---|
| crystal formula | **1j**·(CS$_2$)$_{0.95}$ | **1k**·(CS$_2$)$_{2.1}$ | **1k**·ODCB | **1n**·(PhI)$_{0.5}$ (n-C$_5$H$_{12}$)$_{0.5}$ | **1n**·(2-BrC$_4$H$_3$S) | **1o**·(C$_5$H$_{12}$)$_{0.85}$ (CS$_2$)$_{0.65}$ |
| chemical formula | C$_{201.9}$H$_{90}$O$_{10}$S$_{3.8}$ | C$_{112.1}$H$_{35}$S$_{4.2}$ | C$_{116}$H$_{39}$Cl$_2$ | C$_{105.5}$H$_{53.5}$I$_{0.5}$ | C$_{104.6}$H$_{51.3}$Br$_{0.7}$S$_{0.7}$ | C$_{124.9}$H$_{55.2}$S$_{1.3}$ |
| $M_r$ [g mol$^{-1}$] | 2797.37 | 1516.25 | 1503.37 | 1384.43 | 1386.34 | 1597.37 |
| crystal system[a] | triclinic | triclinic | monoclinic | monoclinic | monoclinic | monoclinic |
| space group | $P\bar{1}$ | $P\bar{1}$ | $P2_1/n$ | $P2_1/n$ | $P2_1/n$ | $P2_1/c$ |
| $a$ [Å] | 16.3105(12) | 16.819(3) | 18.4647(12) | 18.523(2) | 18.556(2) | 22.427(3) |
| $b$ [Å] | 18.6328(14) | 16.962(2) | 18.8691(13) | 15.5501(17) | 15.504(2) | 13.9906(18) |
| $c$ [Å] | 23.6341(17) | 17.234(3) | 20.0169(13) | 23.511(3) | 23.526(3) | 27.122(4) |
| $\alpha$ [°] | 78.1280(10) | 65.404(2) | 90 | 90 | 90 | 90 |
| $\beta$ [°] | 72.8500(11) | 67.535(1) | 94.7280(10) | 108.9990(10) | 110.152(2) | 112.9700(10) |
| $\gamma$ [°] | 73.5040(10) | 67.829(2) | 90 | 90 | 90 | 90 |
| $V$ [Å$^3$] | 6522.2(8) | 3989.3(11) | 6950.4(8) | 6403.0(12) | 6353.7(14) | 7835.2(18) |
| $Z$ | 2 | 2 | 4 | 4 | 4 | 4 |
| $\rho_{calcd}$ [g cm$^{-3}$] | 1.424 | 1.262 | 1.437 | 1.436 | 1.449 | 1.354 |
| $\mu$ [cm$^{-1}$] | 0.145 | 0.178 | 0.156 | 0.319 | 0.542 | 0.110 |
| $F(000)$ | 2884.4 | 1550 | 3076 | 2852 | 2858 | 3302 |
| $2\theta_{min}, 2\theta_{max}$ [°] | 7.64 | 7.68 | 7.58 | 7.62 | 7.64 | 7.60 |
| | 61.30 | 52.96 | 54.10 | 60.14 | 56.74 | 56.72 |
| reflns. collected | 64337 | 30802 | 56074 | 62186 | 78750 | 69265 |
| no. unique reflns. | 35978 | 16020 | 15179 | 18341 | 15787 | 19482 |
| $R_{int}$ | 0.0189 | 0.0471 | 0.0936 | 0.0779 | 0.0554 | 0.0544 |
| obsd. reflns. [$I > 2\sigma(I)$] | 24778 | 8062 | 6766 | 10095 | 10893 | 12129 |
| parameters/restraints | 2022/6 | 1063/6 | 1063/0 | 981/7 | 987/16 | 1091/64 |
| $R_1$, $wR_2$ | 0.1017 | 0.1457 | 0.1264 | 0.1378 | 0.0880 | 0.1323 |
| (obsd. data) | 0.2436 | 0.2559 | 0.1594 | 0.1952 | 0.1438 | 0.2621 |
| $R_1$, $wR_2$ | 0.0748 | 0.0844 | 0.0575 | 0.0706 | 0.0539 | 0.0840 |
| (all data) | 0.2221 | 0.2262 | 0.1392 | 0.1622 | 0.1268 | 0.2264 |
| GOF on $F_o^2$ | 1.134 | 1.043 | 0.822 | 1.030 | 1.027 | 1.021 |
| $\Delta$ [e Å$^{-3}$] | 0.761 | 0.974 | 0.801 | 0.531 | 0.674 | 0.966 |
| | −0.970 | −0.853 | −0.534 | −0.684 | −0.534 | −0.772 |

[a] All data were collected at 100 K.
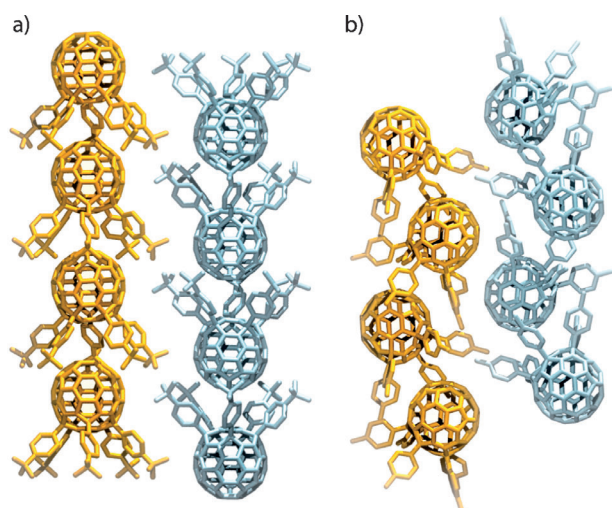
Figure 3. Representative stacking motifs observed in this study: a) Section of the crystal structure of 4-*tert*-butylphenyl derivative **1a**·(PhCl)$_3$ showing two straight-stacked antiparallel columns ($\Theta = 179.4°$). b) Section of the crystal structure of 4-tolyl derivative **1d**·(PhMe)$_3$ showing two zigzag-stacked antiparallel columns ($\Theta = 115.9°$). Hydrogen atoms and solvent molecules are omitted for clarity.

substituents with large sizes and compact shapes (Scheme 2, Table 1). Straight-stacked motifs are observed in crystals obtained from all solvents investigated if the aryl feathers have relatively large substituents at the 4-position, such as in the *tert*-butyl (**1a**) or ketal derivatives (**1e** or **1f**; Figures 3a and 5a–c). On the other hand, rod-shaped feathers tend to produce dimeric or non-stacked motifs even when their substituents are as large as the *tert*-butyl group in 4,4′-*tert*-butylbiphenyl (**1l**; Figure 11a, Table 2). As noted earlier, the potential for a universal straight-stacking motif obtained independently from any solvent of crystallization was central to this project. Accordingly, 4-*tert*-butylphenyl system **1a** is the best example of a universally stacking pentaarylfullerene because it crystallizes in straight-stacked motifs from all solvent systems investigated. Overall, derivatives that crystallize with a straight stacking motif tend not to display any other type of packing motif. This indicates that the stacking interaction is a dominant force for crystallization.

The chlorobenzene solvate of 4-*tert*-butylphenyl system **1a** is the most characteristic example of a straight-stacked packing motif ($\Theta = 179.4°$, Figures 1b and 3a). The straight-stacking preference is induced by the deep and well-defined socket in compound **1a** (Figure 2d), which reduces the number of possible orientations of the nestled fullerene body, that is, the slanting of a fullerene body away from the stack axis may result in unfavorable steric interactions between the *tert*-butyl groups and adjacent pentaarylfullerene carbons within the same stack. The linearity of the stacks appears to be influenced by interactions between occluded interstack solvent molecules; the *n*-pentane solvate gives a less straight stack ($\Theta = 177.8°$, Figures 3a and 4, Table 1) than that of the chlorobenzene solvate.



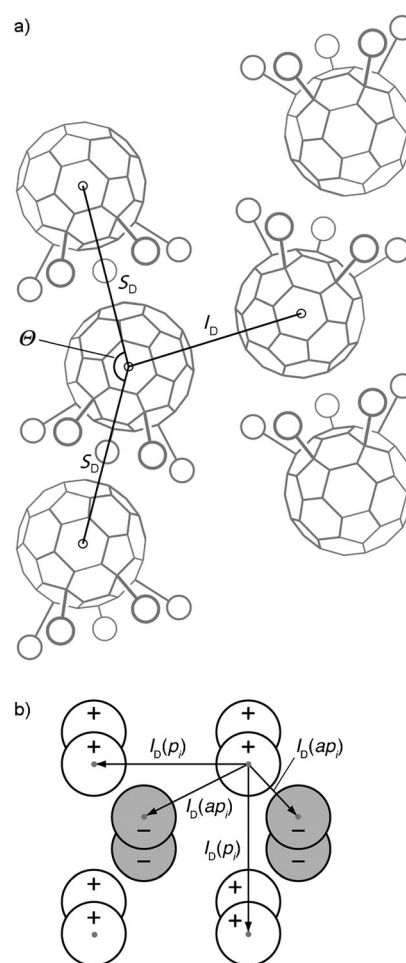Figure 4. Packing parameters in stacked pentaarylfullerenes (**1**). a) Two antiparallel zigzag stacks with defined intrastack angle $\Theta$ [°], intrastack separation $S_D$ [Å], and shortest interstack distances between the centroids[23] of the nearest fullerenes in antiparallel ($I_D(ap_i)$, $i = a, b, c$) or parallel columns ($I_D(p_i)$, $i = a, b, c$) [Å]. b) View down the stack axes. Parallel and antiparallel stacks are denoted with $+$ and $-$ signs.

Fullerene derivatives **1a**, **1b**, and **1e–h** crystallize in straight stacks that tend to pack together inefficiently, requiring a large volume fraction of solvent to fill interstack voids (Figure 5, Tables 1 and 3–5).[25,26] There are significant variations in the parameters within parallel ($I_D(p_a)$, $I_D(p_b)$, $I_D(p_c)$) or antiparallel stacks ($I_D(ap_a)$, $I_D(ap_b)$, $I_D(ap_c)$) and the distribution of cocrystallized solvent molecules (Table 1).

The ODCB solvate of 4-phenoxyphenyl derivative **1h** (Figure 5g) is an exception among straight-stacked systems because it crystallizes with a smaller 1:1 ratio of occluded solvent, presumably due to the conformational flexibility of the *p*-phenoxy substituents, which can occupy space that would otherwise be taken by the solvent of crystallization. Although the parallel ($I_D(p_a) = 13.9$ Å) and antiparallel stacking parameters ($I_D(ap_a) = 17.5$, $I_D(ap_b) = 18.5$, and $I_D(ap_c) = 20.5$ Å) are in the general range of the straight-stacking systems of Table 1, a large volume fraction of the crystal-packing structure is occupied by the phenoxy groups,
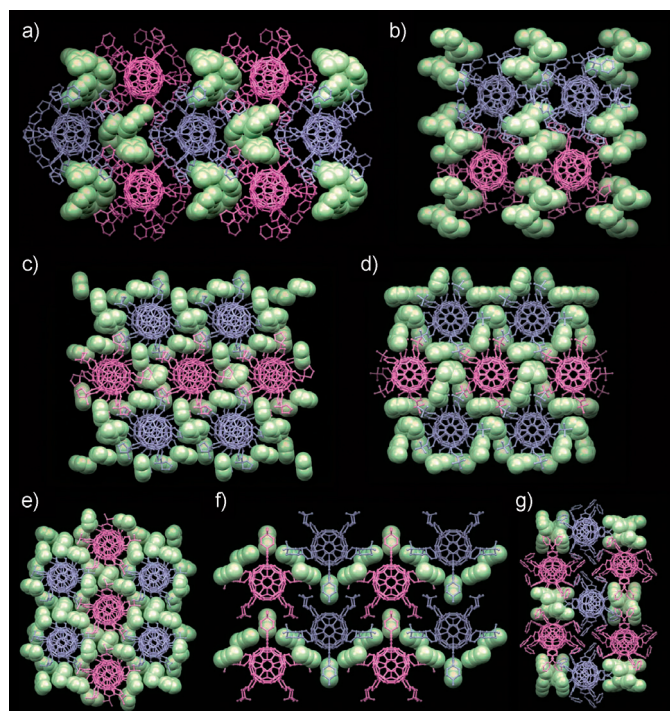
Figure 5. Orthographic projections viewed down the stack axes for the packing motifs of the crystal structures of several straight-stacked pentaarylfullerenes ($\Theta \geq 167°$). a) $\mathbf{1f}\cdot(PhCl)_3$; b) $\mathbf{1f}\cdot(CHCl_3)_{2.5}(Et_2O)_{0.5}$; c) $\mathbf{1e}\cdot(PhMe)_3$; d) $\mathbf{1a}\cdot(PhCl)_3$; e) $\mathbf{1b}\cdot(PhCl)_3$; f) $\mathbf{1g}\cdot(CS_2)_3$; g) $\mathbf{1h}\cdot(ODCB)$. Hydrogen atoms are omitted for clarity and solvent molecules are shown in green space-filling style. Purple and violet colors represent the parallel/antiparallel relationships of the stacks.

which isolate the fullerene π systems between each stack in a manner similar to the other straight-stacked systems.

*Zigzag-stacked systems*: As the size, or more specifically the "cone angle", of the substituent is reduced, for example, in isopropyl system **1b** or acetal derivative **1g**, a zigzag-stacked motif is usually formed in crystals with intrastack angles $\Theta$ as small as 115.9° for *p*-tolyl system $\mathbf{1d}\cdot(PhMe)_3$ (Table 1 and Figures 3b, 6g, and 7). The zigzag-stacked motif for **1d** may be expected on account of the relatively small size of its 4-methyl substituents, which allows a methyl group of each pentakis(4-tolyl)fullerene molecule to slot neatly between two *p*-tolyl groups of the adjacent molecule within the stack (Figure 7). As will be seen below, 4-tolyl derivative **1d** also forms a dimeric motif when it is crystallized from 1-chloronaphthalene/MeOH.

Overall, the wider, less well-defined sockets of pentaarylfullerenes **1b**, **1d**, or **1g** confer greater freedom of movement to the nestled fullerene balls, resulting in a greater sensitivity to the crystallization conditions and often the appearance of several different packing motifs for the same fullerene derivative (Tables 1 and 2). Thus, whereas isopropyl derivative **1b** forms a straight-stacked motif when crystallized from chlorobenzene, a zigzag-stacked motif is obtained when the compound is crystallized from 1-chloronaphthalene/*n*-pentane (Figure 6c) or ODCB/*n*-hexane (Fig-
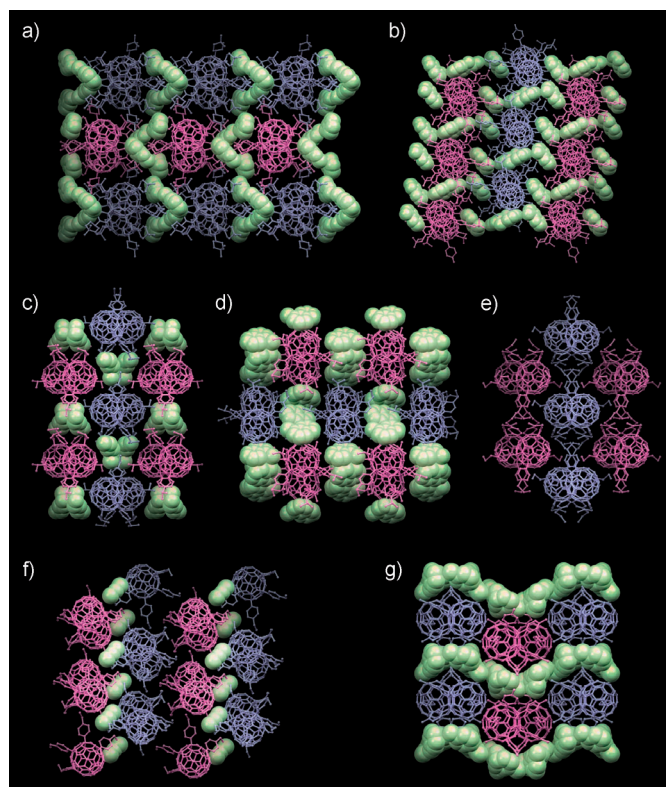


Figure 6. Orthographic projections viewed down the stack axes for the packing motifs of the crystal structures of several zigzag-stacked pentaarylfullerenes sorted in order of decreasing aryl substituent size: a) $\mathbf{1g}\cdot(PhOMe)_2$; b) $\mathbf{1g}\cdot(1\text{-ClNp})_2$; c) $\mathbf{1b}\cdot(1\text{-ClNp})_2$; d) $\mathbf{1b}\cdot(n\text{-}C_6H_{14})_{0.5}$-$(ODCB)_{0.5}$; e) $\mathbf{1i}$ (no solvent); f) $\mathbf{1c}\cdot(CS_2)_{0.5}$; g) $\mathbf{1d}\cdot(PhMe)_3$. Hydrogen atoms are omitted for clarity and solvent molecules are shown in green space-filling style. Purple and violet colors represent the parallel/antiparallel relationships of the stacks.
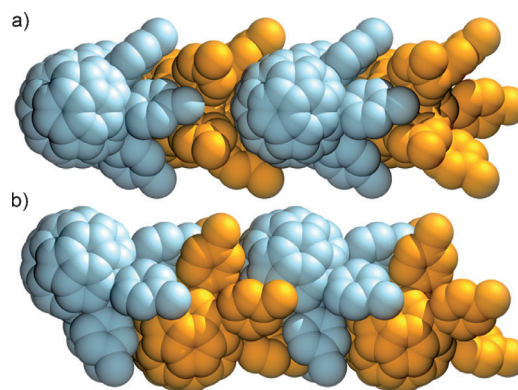


Figure 7. Space-filling representations of the crystal structure of solvate $\mathbf{1d}\cdot(PhMe)_3$. View along a) the *b* axis and b) the *a* axis. Hydrogen atoms and solvent molecules are omitted for clarity.

ure 6d), whereas a non-stacking motif is formed when the compound is crystallized from carbon disulfide (Figure 18). Similarly, acetal derivative **1g** forms different stacking motifs when crystallized from carbon disulfide (straight), anisole (zigzag), or 1-chloronaphthalene (zigzag; Table 1, Figures 5f and 6a,b).

The centroid-to-centroid distances, $S_D$, between adjacent fullerene bodies within a stack are all ca. 11 Å, whether they are straight- or zigzag-stacked (Table 1). Interestingly, the dominant interactions between molecules within a stack are due to *ortho*- and *meta*-hydrogen atoms of 1,4-phenylene groups clashing into $C_{60}$ carbons of an adjacent pentaarylfullerene (Figure 8a).[14] These interactions prevent any of the fullerene carbon atoms from coming into van der Waals contact with either the hydrogen or carbon atoms of the fullerene-embedded cyclopentadiene on an adjacent molecule (socket). For example, H1 in Figure 8c,d does not come into direct contact with any of the $C_{60}$ carbons of the adjacent fullerene core (Figure 8c, left), as judged from the relatively large H1···C31 distance of 3.733(2) Å. In fact, all intermolecular H1···C distances are above the van der Waals contact distance of 2.8 Å in the crystal structures in which the hydrogen atom could be unambiguously located ($1c·(CS_2)_{0.5}$, $1f·(CHCl_3)_{2.5}(Et_2O)_{0.5}$, $1g·(CS_2)_3$, $1g·(1-ClNp)_2$, and $1i$).

In stark contrast, the non-arylated zigzag-stacked 6,9,12,15,18-pentamethyl-1-hydro[60]fullerene (1, R = $CH_3$)[19a] has a relatively short intermolecular distance of 2.74 Å between the fullerene-embedded cyclopentadiene H6 and carbon C32 of an adjacent fullerene, which places these two atoms in direct contact (Figure 8b). Similarly, cyclopentadienyl carbon C7 also lies in close contact with C32 (3.382(4) Å). Two pairs of fullerene carbons between adjacent stacks (C15···C23 and C16···C23) have also short contact distances of 3.312(4) and 3.367(4) Å, respectively.[19a] These data indicate that replacing the aryl addends in pentaarylfullerenes 1a–o with smaller groups can in some instances lead to tightly stacked motifs, which may be a way of enhancing the electron mobility of $C_{60}$ derivatives with the 1,6,9,12,15,18-substitution pattern in OPVDs. This aspect will be explored in future work.

In summary, the fullerene π systems in all stacked pentaarylfullerene derivatives do not come into direct van der Waals contact, which is likely to significantly hinder electronic interactions along a stack. Furthermore, the π surfaces of fullerene units within straight-stacked motifs are completely isolated from those of adjacent stacks, that is, the $I_D(p_i)$ or $I_D(ap_i)$ interstack distances are relatively large and range from around 14 to 23 Å (Table 1). This is in part related to the large volume fraction of occluded solvents, mentioned above, and the large bulk of the addends, which induces the straight-stacking motif (Figure 5). On the other hand, when pentaarylfullerenes form zigzag stacks as in $1b·(1-ClNp)_2$, $1b·(n-C_6H_{14})_{0.5}$-$(ODCB)_{0.5}$, $1c·(CS_2)_{0.5}$, $1d·(PhMe)_3$, $1g·(PhOMe)_2$, $1g·(1-ClNp)_2$, and $1i$, several fullerene $sp^2$ carbons come into close contact with fullerene $sp^2$ carbons of adjacent stacks.[14] In most cases, however, because these are discreet interactions, there are no extended networks of contacts. The exceptions are
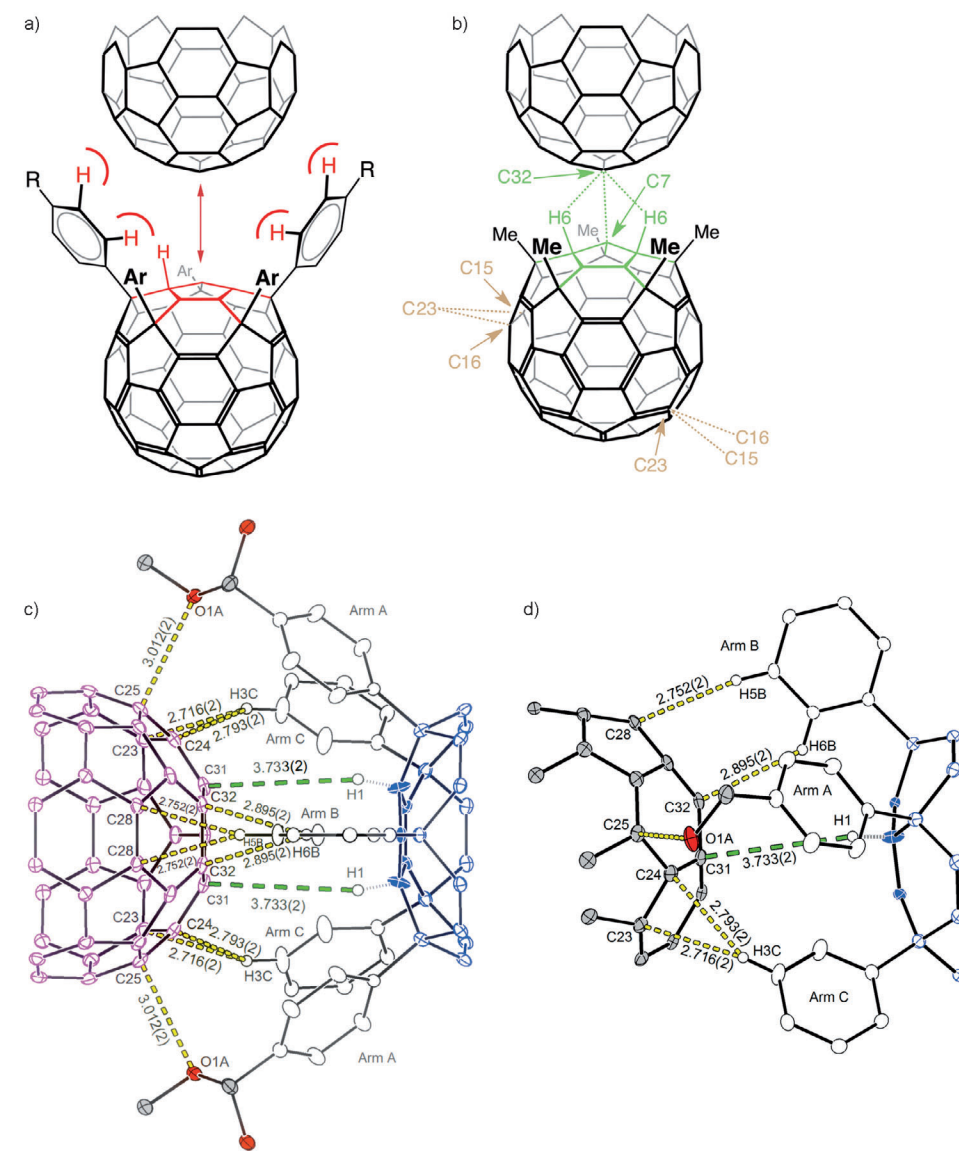


Figure 8. a) Representation of the major intermolecular interactions existing between molecules of pentaarylfullerenes in straight or zigzag stacks, exemplified by acetal system $1g·(CS_2)_3$ in c) and d). b) Representation of the van der Waals interactions within stacks of $C_{60}Me_5H·n$-pentane (ref. [19a]) shown for comparison. c) View along the plane formed by Arm B (along the crystallographic mirror plane) for acetal $1g·(CS_2)_3$ and d) perpendicular view.

for 4-thioethylphenyl derivative **1i** and 4-ethylphenyl derivative **1c**·(CS$_2$)$_{0.5}$, which have small, rod-shaped substituents on the aryl groups and low solvent-to-fullerene ratios (Figure 6e, f). Of these two, compound **1i** forms a continuous one-dimensional network of close contacts (Figure 9a), whereas compound **1c**·(CS$_2$)$_{0.5}$ forms discreet one-dimensional clusters containing four pentaarylfullerenes (Figure 9b).[14]

Thioethyl derivative **1i** (Figure 6e) produces a solvent-free zigzag-stacked motif when crystallized from a number of solvent systems. Interestingly, the crystal structure is almost identical to that of the 4-n-propylphenyl derivative reported by Bouwkamp and Meetsma,[27] yet it differs remarkably from 4-ethoxyphenyl derivative **1j**, described below, even though all three compounds are essentially isostructural. Derivative **1i** packs very efficiently in crystals,

creating a continuous one-dimensional network of short intermolecular C···C contacts (Figure 10). In principle, these short contacts could make thioethyl derivative **1i** an excellent candidate for efficient BHJ OPVDs. Unfortunately, the efficient packing of thioethyl system **1i** also renders it poorly soluble in all solvents, making BHJ device preparation by spin casting problematic.

In the context of BHJ OPVDs, a higher fullerene density and a higher number of fullerene π–π contacts in the solid state should increase electron mobility values in the active layer.[13] As mentioned earlier, however, other key factors affect the morphology of the active layer, which may domi-



Figure 9. Representations of the one-dimensional networks of close contacts between fullerene carbons in a) 4-thioethylphenyl system **1i** and b) 4-ethylphenyl system **1c**·(CS$_2$)$_{0.5}$. Short contact distances were obtained from fullerene centroid-to-centroid distances of ≤ 10.5 Å. Aryl addends, except for *ipso* carbons, are not shown for clarity. Fullerene-embedded cyclopentadienyl rings are shown as filled ellipsoids.
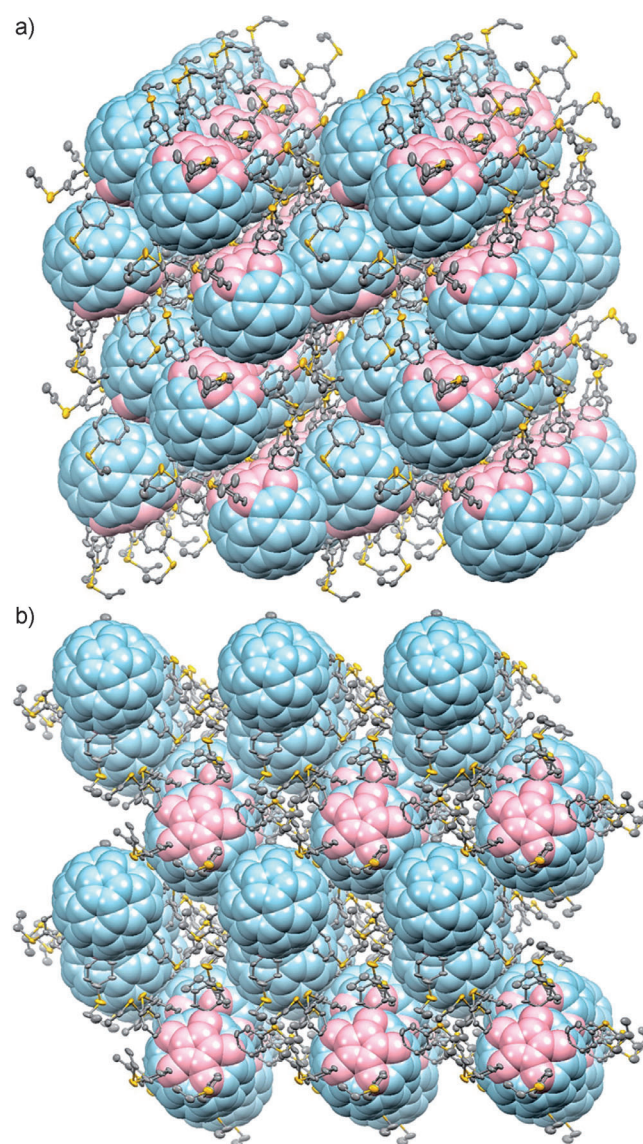


Figure 10. Representations of the solvent-free crystal structure of 4-thioethylphenyl system **1i**: View along a) the *a* axis and b) the *c* axis, both with a slight offset. Hydrogen atoms are omitted for clarity. The sixty carbons of the fullerene units are represented in space-filling mode and the aryl substituents in ORTEP mode with thermal ellipsoids at 50% probability. The fullerene-embedded cyclopentadiene ring and adjacent carbons of the fullerene units are shown in pink.

nate the performance of BHJ OPVDs.[9] In general for all the pentaarylfullerenes in this study, the overall fullerene density, that is, the number of pentaarylfullerene molecules per volume in the unit cell, increases as the size of the aryl group decreases and, to a lesser extent, as the solvent-to-fullerene ratio decreases. Accordingly, benzophenone ketal derivative $1f\cdot(PhCl)_3$ has the lowest fullerene density ($3.8 \times 10^{-4}$ Å$^{-3}$) and 4-ethylphenyl derivative $1c\cdot(CS_2)_{0.5}$ has the highest ($6.8 \times 10^{-4}$ Å$^{-3}$) of all the stacking pentaarylfullerene derivatives **1a–i** (Table 1).

*Dimeric motifs*: The group of Matsuo and Nakamura first reported an interdigitated dimeric motif in crystals of the 4-(*n*-hexyldimethylsilylethynyl)phenyl derivative (**1**, R = 4-([*n*-C$_6$H$_{13}$]Me$_2$SiC≡C)C$_6$H$_4$).[28] In fact, the presence of rod-shaped addends on the pentaarylfullerene framework generally favors the formation of a dimeric motif in the solid state, as judged from the results below.

4-*tert*-Butylbiphenyl derivative **1l** produces a face-to-face dimeric motif in which the *tert*-butyl groups mesh together in a gear-like fashion when crystallized from a number of solvent systems (Figure 11a,b). In the beautiful crystal structure of $1l\cdot(c\text{-}C_6H_{12})_4$, a cluster of six close-packed cyclohexane molecules is encapsulated within the large cavity created between the two fullerene molecules (Figure 11a). The resulting lozenge-shaped dimers pack efficiently in the crystal (Figure 11b), which may explain why this is the only packing motif observed regardless of the crystallization solvent.

When 4-tolyl derivative **1d** is crystallized from 1-chloronaphthalene/MeOH, a face-to-face dimeric motif is observed in which a disordered methanol molecule resides in the cavity formed between the two pentaarylfullerenes (Figure 11c, Table 2). This motif contrasts with the zigzag stacking behavior of 4-tolyl derivative **1d** as a solvate with toluene or ODCB/*n*-pentane (Figures 3b, 6g, and 7 and Table 1).[29] It is possible that a dimeric motif is not observed with toluene or ODCB/*n*-pentane because these solvents are too large to fit in the cavity.

The crystal structures of 4-ethoxy solvates **1j**·PhMe and $1j\cdot(CS_2)_2$ form the same dimeric motif in which the ethoxy groups are interdigitated (Figures 11d and 12, Table 2). The ethoxy groups fit tightly together and form a circular array of twelve short contacts (Figure 12). This array is composed of eight interactions between methylene hydrogen atoms and neighboring phenoxy oxygen atoms, and four others between *ortho* aryl hydrogen atoms and neighboring phenoxy oxygen atoms. A similar dimeric motif is not possible with thioethyl derivative **1i** described above, or with Bouwkamp's 4-*n*-propylphenyl derivative[27] because the sulfur atoms or methylene groups are too large to accommodate similar close-contact interactions.

The relatively small size of the ethoxy groups of compound **1j**, as well as the nature of the dimeric motif that exposes the maximum possible area of the C$_{60}$ surface, instigate complex three-dimensional networks of close contacts between fullerene units in the solid state. In the crystal
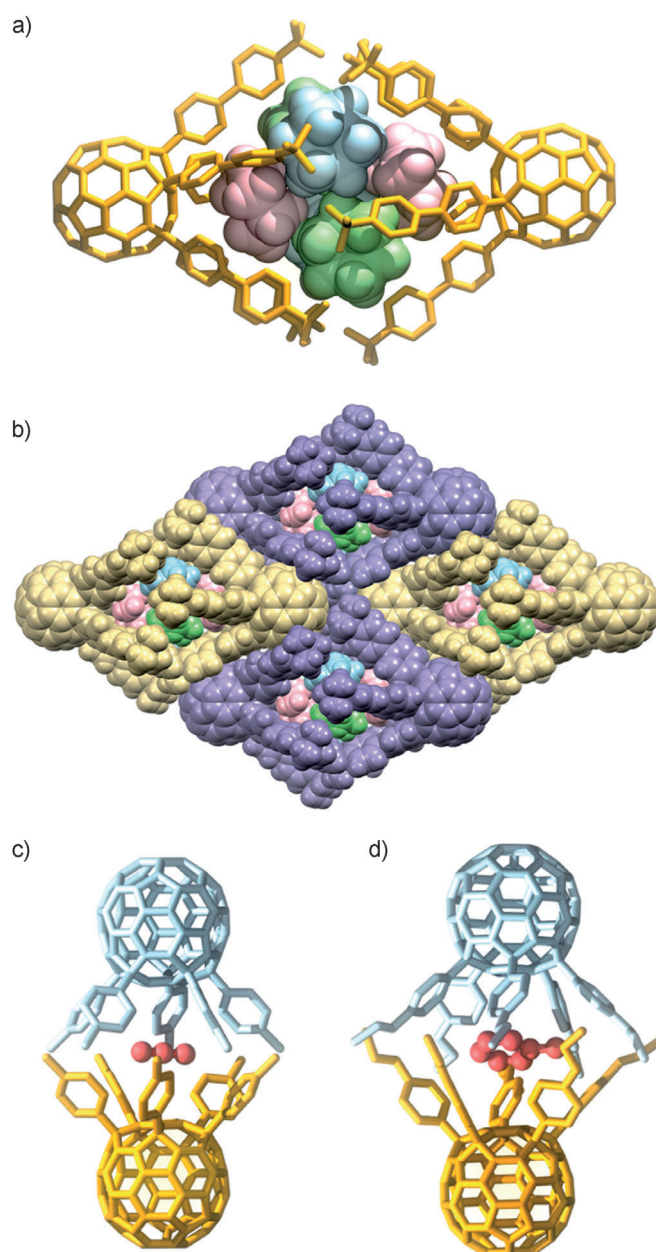


Figure 11. Examples of dimeric motifs for a) $1l\cdot(c\text{-}C_6H_{12})_4$, c) $1d\cdot(1\text{-}ClNp)(MeOH)_{0.5}$, and d) **1j**·PhMe. b) Crystal-packing structure of $1l\cdot(c\text{-}C_6H_{12})_4$ with two interstitial (outside the dimer cavity) cyclohexane molecules per unit cell omitted for clarity. Except for b), all hydrogen atoms are omitted for clarity and solvent molecules are shown in space-filling or ball-and-stick style. The occluded methanol molecule in c) is disordered over two positions.

structure of solvate **1j**·PhMe (Figure 13a,b), each pentaarylfullerene has four near neighbors and produces a three-dimensional network of close contacts. This network has a slightly higher density of close contacts than in the two-dimensional network of solvate $1j\cdot(CS_2)_2$ (Figure 13c,d), in which each pentaarylfullerene has an average of 3.5 near neighbors.

A spectacular case of dimer formation was found for 2-naphthyl derivative **1k** (Figure 14). On the basis of comput-
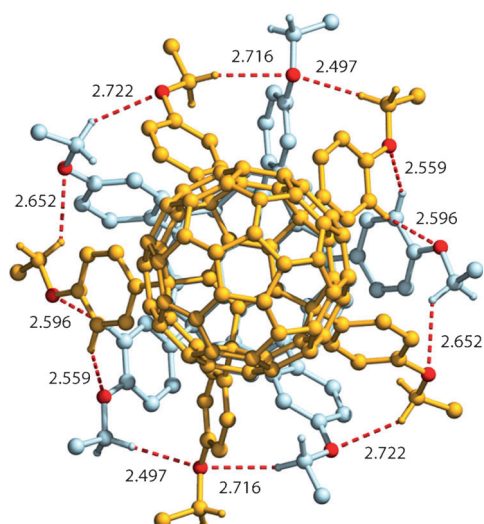
Figure 12. Ball-and-stick representation of a dimeric unit in the crystal structure of solvate $1j\cdot(CS_2)_2$. The twelve dashed connectivities represent interatomic distances [Å] within the sum of van der Waals radii of oxygen and hydrogen atoms.
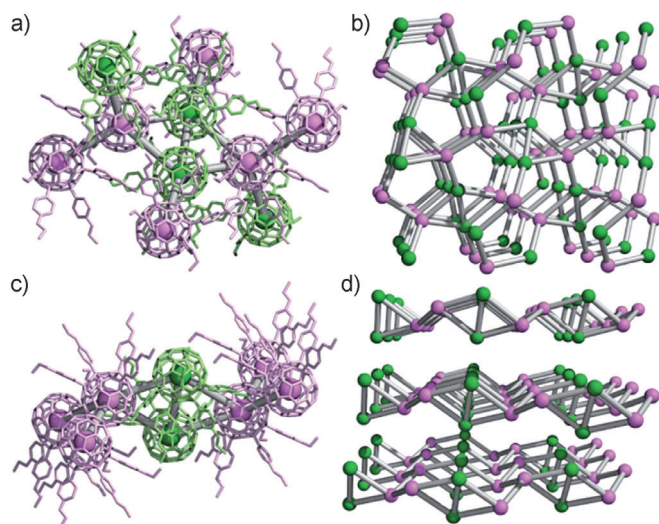


Figure 13. Ball-and-stick representations of the close-contact networks within the crystal structures of a),b) $1j\cdot(PhMe)$ and c),d) $1j\cdot(CS_2)_2$. Views a) and c) represent small sections of the extended close-contact networks shown in b) and d), respectively. Solid spheres, drawn with an arbitrary radius of 1.7 Å, represent the centroids of the $C_{60}$ cages. Grey connectivity spokes represent centroid-to-centroid distances of ≤10.5 Å. The green and pink colors indicate symmetry-independent pentaarylful-lerenes with different close-contact environments. For clarity, the pen-taarylfullerene molecules, which are represented by green and pink con-nectivities in a) and c), are omitted in the extended networks b) and d).

er modeling (Figure 2c), compound **1k** was expected to pack in a head-to-tail fashion to form a robust stacking motif. Instead, the crystal structures of $1k\cdot(ODCB)_{1.5}$, $1k\cdot(CS_2)_5$, and $1k\cdot(CH_2I_2)_x$ all contain a face-to-face dimeric motif (Figures 14 and 15). In these structures, each pentaar-ylfullerene is paired with its conformational enantiomer through a crystallographic inversion center (Figure 14a).
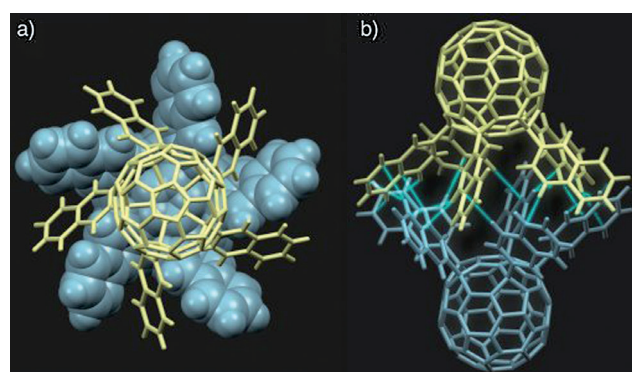


Figure 14. Representations of the dimeric motif created by C−H···π inter-actions between 2-naphthyl units $1k\cdot(CS_2)_5$ in the crystal. a) View down the quasi-fivefold axis of the complex and b) side-view showing the C−H···π interactions in aquamarine. The occluded $CS_2$ solvent molecule is omitted for clarity.
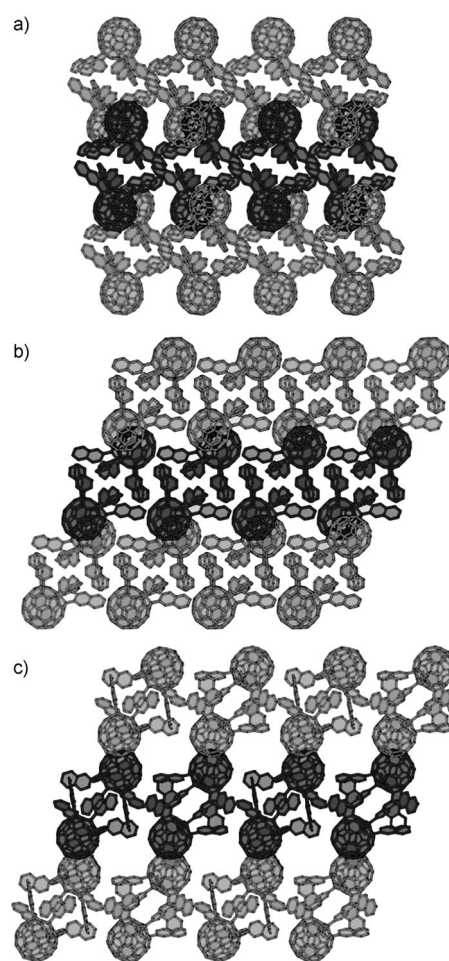


Figure 15. Representations of the crystal structures of $1k\cdot(ODCB)_{1.5}$, $1k\cdot(CS_2)_5$, and $1k\cdot(CH_2I_2)_x$. a) $1k\cdot(ODCB)_{1.5}$ viewed down the $b$ axis. b) $1k\cdot(CS_2)_5$ viewed along the (01−1) vector. c) $1k\cdot(CH_2I_2)_x$ viewed along the (01−1) vector with solvent channels clearly visible. Hydrogen atoms and solvent molecules are omitted for clarity.

The 2-naphthyl groups are arranged like the blades of a pro-peller, with each group participating in an edge-to-face C−

H···π interaction as both a donor and an acceptor (Figure 14b). This unusual network of cooperative C−H···π interactions appears to strongly promote dimerization in the three crystallization solvent systems investigated. In each case, a solvent molecule is encapsulated within the cavity created between the two pentaarylfullerenes.

The increasing ratio between cocrystallized solvent and pentaarylfullerene molecules across the series **1k**·(ODCB)$_{1.5}$ to **1k**·(CS$_2$)$_5$ to **1k**·(CH$_2$I$_2$)$_x$ is reflected in the decreasing fullerene density and lower dimensionality of the networks of close contacts between fullerene units ($\rho_F = 6.08$, 5.99, and $5.76 \times 10^{-4}$ Å$^{-3}$, respectively, Table 2). Accordingly, **1k**·(ODCB)$_{1.5}$ forms a two-dimensional close contact network, whereas **1k**·(CS$_2$)$_5$ and **1k**·(CH$_2$I$_2$)$_x$ both form one-dimensional networks (Figure 15a–c).

*Non-stacked systems*: Several pentaarylfullerenes (**1m–o**) with substitution at the 3-position of the phenylene rings were also investigated (Scheme 1). Molecular modeling suggested that any of the 3-substituted phenyl systems in this study could form stacking motifs with C$_{60}$ centroid-to-centroid distances of around 11 Å, even in cases of pentaarylfullerenes with small (**1m–o**) or very large sterically demanding aryl groups (e.g., 4-tritylphenyl or 3,4-di-*tert*-butylphenyl; not shown in Figure 2). Experimentally, however, none of the 3-substituted phenylene systems form stacking motifs (Table 2).[22] It is possible that the socket produced by the aryl feathers is too shallow and that the cumulative van der Waals forces are not large enough to stabilize a stacking motif relative to a non-stacked one.

Three different non-stacking motifs are formed with the five solvent systems used to crystallize 3-tolyl derivative **1m** (Table 2).[8,22] A solvent molecule resides within the bowl of 3-tolyl derivative **1m** in each case (not shown), but the packing structures and networks of close contacts between fullerene moieties are very different.[8] Crystals of **1m**·CS$_2$ and **1m**·CHCl$_3$ have an identical diamond-like network of close contacts in which each pentaarylfullerene has four near neighbors arranged in an approximately tetrahedral geometry (Figure 16a, b and Table 2). On the other hand, crystals of **1m**·PhMe (Figure 16c, d) and **1m**·ODCB (not shown) form similar layered extended networks of close contacts in which the pentaarylfullerene molecules are approximately hexagonally close-packed and each pentaarylfullerene is surrounded by five near neighbors. A third motif is observed for solvate **1m**·(PhCl)$_2$ (Figure 16e, f). Here the ratio of solvent to pentaarylfullerene is greater and there is correspondingly a less dense, layered, honeycomb-like network of close contacts, in which each pentaarylfullerene has only three near neighbors. Although it is unclear why chlorobenzene would induce a different packing motif than that found for toluene or ODCB, these results indicate that 3-tolyl fullerene derivative **1m** is very sensitive to the conditions of crystallization. Compounds **1m**·CS$_2$ and **1m**·CHCl$_3$ have the highest overall fullerene packing densities found in this study as a result of the small size of the aryl substituent in combination with the small ratio of occluded solvent, with
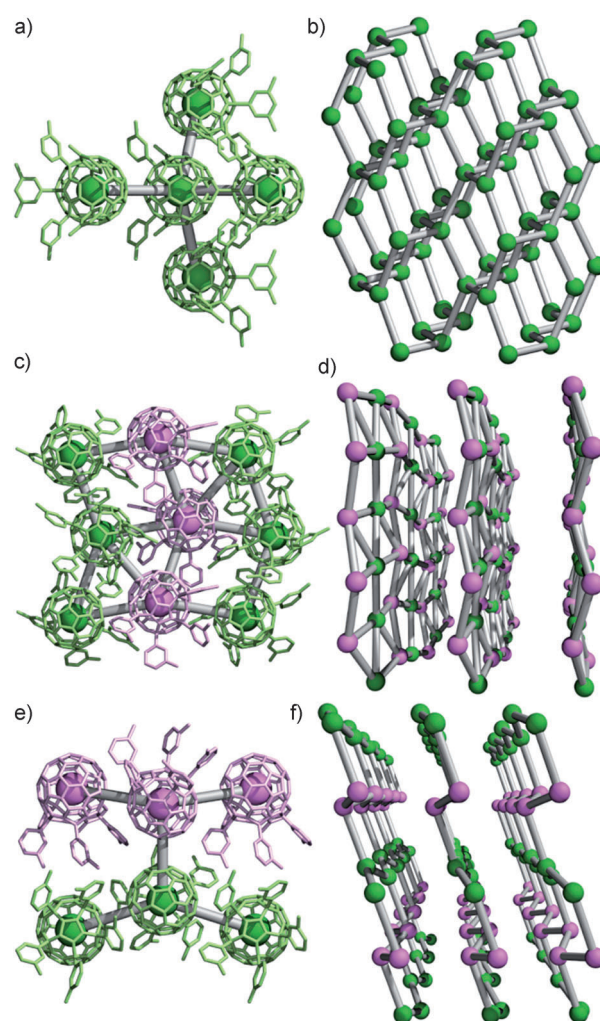


Figure 16. Close-contact networks for the crystal structures of a), b) **1m**·CHCl$_3$, c), d) **1m**·PhMe, and e), f) **1m**·(PhCl)$_2$. Views a), c), and e) represent small sections of the extended close-contact networks shown in b), d), and f), respectively. Solid spheres, drawn with an arbitrary radius of 1.7 Å, represent the centroids of the C$_{60}$ cages. Grey connectivity spokes represent centroid-to-centroid distances of ≤10.5 Å. Green and pink colors indicate symmetry-independent pentaarylfullerenes with different close-contact environments. For clarity, the pentaarylfullerene molecules, which are represented in green and pink in a), c), and e) are omitted in the extended networks b), d), and f).

compound **1m**·(PhCl)$_2$ having the lowest value of these three motifs ($\rho_F = 7.02$, 7.01, and $6.78 \times 10^{-4}$ Å$^{-3}$, respectively, Table 2).

*meta*-Xylyl system **1n** was also found to have a peculiar crystal-packing behavior. Similarly to 4-*tert*-butylbiphenyl system **1l** (Figure 11a), the crystal structure of compound **1n**·(*c*-C$_6$H$_{12}$)$_4$ is dominated by cocrystallized cyclohexane molecules (Figure 17) and the pentaarylfullerene molecules form discreet side-to-side dimers that are fully isolated from other dimeric units by the occluded cyclohexane molecules.

On the other hand, the crystal structures of 3,5-xylyl systems **1n**·(PhI)$_{0.5}$(*n*-C$_5$H$_{12}$)$_{0.5}$ and **1n**·(2-BrC$_4$H$_3$S)$_{0.7}$(*n*-C$_6$H$_{14}$)$_{0.3}$ form essentially identical feather-in-cavity motifs, in which a methyl group of the substituent is directed into the cavity
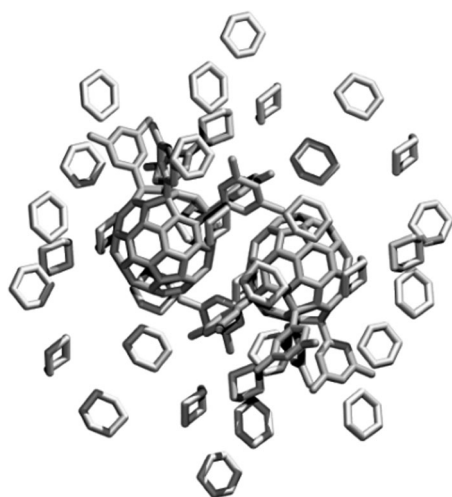
Figure 17. Representation of the crystal structure of **1n**·($c$-$C_6H_{12}$)$_4$. A discreet side-to-side dimer of pentaarylfullerenes is surrounded by a number of cyclohexane molecules.

of an adjacent fullerene molecule to form a zigzag chain of feather-in-cavity interactions (Figure 18a, b). Compared to solvate **1n**·($c$-$C_6H_{12}$)$_4$, this packing motif is more efficient and requires only one solvent molecule per fullerene molecule. Correspondingly, there is a two-dimensional close-contact network (Figure 18c). A similar feather-in-cavity motif is seen in crystals of 4-isopropylphenyl system **1b**·$CS_2$ (Figure 18d, e). In this case, the fullerene packing density is
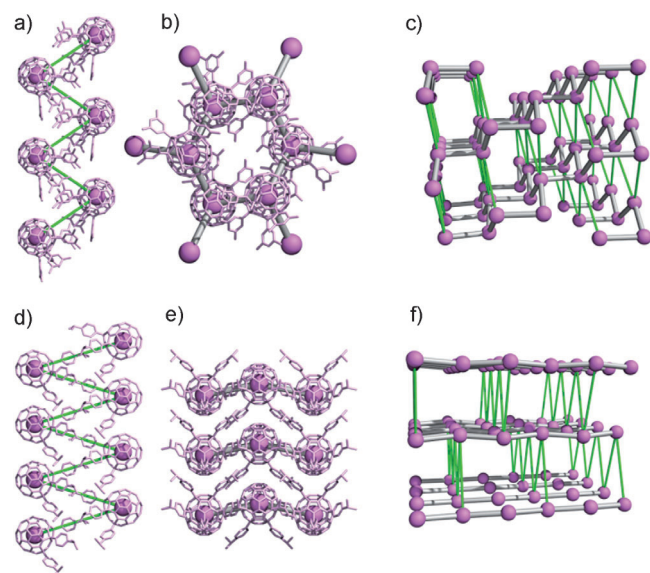


Figure 18. a) Representation of the crystal structures of a)–c) compound **1n**·(PhI)$_{0.5}$($n$-$C_5H_{12}$)$_{0.5}$, and d)–f) **1b**·$CS_2$. Views a), b) and d), e) represent small sections of the close-contact networks shown in c) and f), respectively. In all cases, pink spheres, which are drawn with an arbitrary radius of 1.7 Å, represent the centroids of the $C_{60}$ cages. Green connectivity spokes represent feather-in-cavity interactions. Grey connectivity spokes represent centroid-to-centroid distances of $\leq$10.5 Å. For clarity, the pentaarylfullerene molecules, which are represented in pink in a), b), d), and e), are omitted in the extended networks in c) and f).
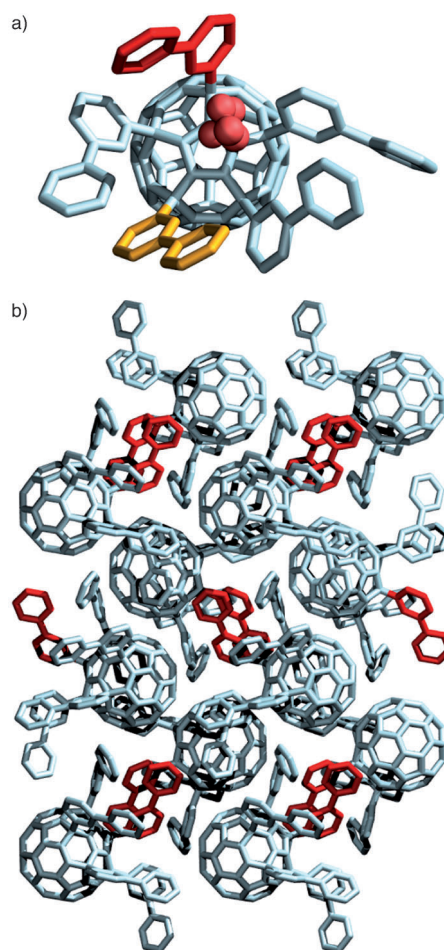


Figure 19. Representations of the crystal structure of compound **1o**·($CS_2$)$_{0.5}$($n$-$C_5H_{12}$)$_{0.5}$. a) Single molecule showing an $n$-pentane molecule within a shallow cavity (red spheres). b) A single $bc$ layer, viewed just off the $a$ axis, showing the $m$-biphenyl π–π interactions in red.

lower and results in a one-dimensional network of close contacts (Figure 18f).

3-Biphenyl derivative **1o** is another unusual pentaarylfullerene because it has a large range of conformations available for each of its biaryl groups and it crystallizes in a non-stacking motif (Figure 19). In the crystal structure of compound **1o**·($CS_2$)$_{0.5}$($n$-$C_5H_{12}$)$_{0.5}$, one of the biphenyl groups (Figure 19, shown in yellow) is directed towards the embedded cyclopentadiene ring, whereas another biphenyl group (Figure 19, shown in red) participates in a π–π aromatic ring pairing interaction with a biphenyl group of a neighboring pentaarylfullerene. The resulting cavity is small and narrow and contains a cocrystallized $n$-pentane molecule in an approximately all-*anti* conformation (red spheres). The fullerene units are arranged in such a way as to produce a puckered, honeycomb-like network of close contacts with cocrystallized $CS_2$ and $n$-pentane molecules situated between pentaarylfullerene layers (not shown).

## Conclusion

We have shown that relatively small changes in molecular shape through variation of the size of the five substituents in pentaarylfullerene systems **1a–o** can greatly influence the packing motifs of these molecules in terms of their relative orientations and the densities of the close-contact networks they form in the crystal. Accordingly, straight and zigzag-stacking motifs can be reliably obtained in crystalline solids. In some cases, the crystallization solvent has a strong influence on the crystal structure, but in many cases the structural motifs are essentially solvent-independent (universal stackers). Although the size of the substituent at the 4-position of the aryl addend determines the probability that a stacked motif will be present in the crystal structure, with bulky substituents favoring straight stacking, substituent size has no significant influence on the intrastack separation. Indeed, significant variations in intrastack separation ($S_D$) can occur for the same compound depending on the cocrystallized solvent, for example, 10.787 Å for **1g**·(CS$_2$)$_3$ and 11.396 Å for **1g**·(PhOMe)$_2$. In the majority of cases, the solvent regions within the crystal lattices are highly disordered and there are no specific fullerene–fullerene interactions to direct the crystallization process between stacks. Furthermore, in cases of pentaarylfullerenes with relatively small substituents, especially with the 3-phenyl substitution category, predicting the observed packing motifs is not feasible.

Interestingly, this behavior can be compared to that in the 2D regime, in which C$_{60}$ derivatives form extended structures of fullerene networks through nonbonded interactions with an underlying monolayer of π-conjugated host molecules.[30] In the 3D regime, our work shows that if a fullerene derivative has a high propensity to self-assemble (e.g., **1a**), the occluded solvent molecules are best regarded as guests in a defined host framework, and they contribute only indirectly to the self-assembly process. However, if the interactions between the fullerene derivatives are weaker, a variety of networks can be produced in which the distinction between host and guest is not well defined.

The crystal structures of the pentaarylfullerene molecules reveal significant steric interactions between the *meta* and, to a lesser extent, *ortho* hydrogen atoms of aryl groups and the adjacent stacked fullerene moiety, which prevent the formation of an ideal bowl-shaped cavity (Figure 8).[14] Furthermore, the aryl groups can be oriented in a highly unfavorable manner by being coplanar with the molecular quasi-five-fold mirror plane of the fullerene core, which greatly reduces the size and depth of the socket. In addition, although a robust straight-stacking motif is promoted by increasing the size of the aryl *para*-substituents, individual fullerene cages become increasingly isolated and the corresponding fullerene packing densities in the crystal decrease. In most cases, the crystal structures that display a straight-stacking motif contain a much larger volume fraction of cocrystallized solvent due to the shape mismatch between robust columns. Reducing the size of the feathers results in shallower and, therefore, less accommodating cavities, which in turn give alternative packing motifs that often depend on the conditions of crystallization.

All of the pentaarylfullerenes described in this work have essentially identical electronic properties in terms of their frontier molecular orbitals. Thus, they are excellent candidates for exploring the effect of crystal packing on OPVD performance.[9] On the other hand, because the fullerene π surfaces of straight-stacked 6,9,12,15,18-pentaaryl-1-hydro[60]fullerenes (**1**) are relatively isolated and are not able to interact well in crystalline solids, it will be highly desirable to trade the six-membered nonheterocyclic aryl addends for smaller groups with or without π surfaces, while keeping the self-assembly concept intact. Further developments in the synthetic methods to obtain these compounds are needed to provide access to a wider range of five- or six-membered heterocyclic analogues of **1** that should not display steric clashes, unlike those found in the *p*-alkylphenyl series. Other strategies could involve different multiaddition patterns on C$_{60}$ as a means of altering the molecular shape and the electronic structure of the fullerene derivative.[2k,l,10c,31]

[1] a) G. Dennler, M. C. Scharber, C. J. Brabec, *Adv. Mater.* **2009**, *21*, 1323–1338; b) B. C. Thompson, J. M. J. Fréchet, *Angew. Chem.* **2008**, *120*, 62–82; *Angew. Chem. Int. Ed.* **2008**, *47*, 58–77; c) R. Kroon, M. Lenes, J. C. Hummelen, P. W. M. Blom, B. de Boer, *Polym. Rev.* **2008**, *48*, 531–582.

[2] a) C. J. Brabec, A. Cravino, D. Meissner, N. S. Sariciftci, M. T. Rispens, L. Sanchez, J. C. Hummelen, T. Fromherz, *Thin Solid Films* **2002**, *403–404*, 368–372; b) M. M. Wienk, J. M. Kroon, W. J. H. Verhees, J. Knol, J. C. Hummelen, P. A. van Hal, R. A. J. Janssen, *Angew. Chem.* **2003**, *115*, 3493–3497; *Angew. Chem. Int. Ed.* **2003**, *42*, 3371–3375; c) L. M. Popescu, P. van 't Hof, A. B. Sieval, H. T. Jonkman, J. C. Hummelen, *Appl. Phys. Lett.* **2006**, *89*, 213507; d) S. A. Backer, K. Sivula, D. F. Kavulak, J. M. J. Fréchet, *Chem. Mater.* **2007**, *19*, 2927–2929; e) F. B. Kooistra, J. Knol, F. Kastenberg, L. M. Popescu, W. J. H. Verhees, J. M. Kroon, J. C. Hummelen, *Org. Lett.* **2007**, *9*, 551–554; f) M. Lenes, G.-J. A. H. Wetzelaer, F. B. Kooistra, S. C. Veenstra, J. C. Hummelen, P. W. M. Blom, *Adv. Mater.* **2008**, *20*, 2116–2119; g) Y. Matsuo, Y. Sato, T. Niinomi, I. Soga, H. Tanaka, E. Nakamura, *J. Am. Chem. Soc.* **2009**, *131*, 16048–16050; h) R. B. Ross, C. M. Cardona, D. M. Guldi, S. G. Sankaranarayanan, M. O. Reese, N. Kopidakis, J. Peet, B. Walker, G. C. Bazan, E. V. Keuren, B. C. Holloway, M. Drees, *Nature Mater.* **2009**, *8*, 208–212; i) P. A. Troshin, H. Hoppe, J. Renz, M. Egginger, J. Yu. Mayorova, A. E. Goryachev, A. S. Peregudov, R. N. Lyubovskaya, G. Gobsch, N. S. Sariciftci, V. F. Razumov, *Adv. Funct. Mater.* **2009**, *19*, 779–788; j) G. Zhao, Y. He, Y Li, *Adv. Mater.* **2010**, *22*, 4355–4358; k) A. Varotto, N. D. Treat, J. Jo, C. G. Shuttle, N. A. Batara, F. G. Brunetti, J. H. Seo, M. L. Chabinyc, C. J. Hawker, A. J. Heeger, F. Wudl, *Angew. Chem.* **2011**, *123*, 5272–5275; *Angew. Chem. Int. Ed.* **2011**, *50*, 5166–5169; l) M. Murata, Y. Morinaka, Y. Murata, O. Yoshikawa, T. Sagawa, S. Yoshikawa, *Chem. Commun.* **2011**, *47*,

7335–7337; m) C.-P. Chen, Y.-W. Lin, J.-C. Horng, S.-C. Chuang, *Adv. Eng. Mater.* **2011**, *1*, 776–780.

[3] a) Y. He, Y. Li, *Phys. Chem. Chem. Phys.* **2011**, *13*, 1970–1983; b) C.-Z. Li, H.-L. Yip, A. K.-Y. Jen, *J. Mater. Chem.* **2012**, *22*, 4161–4177.

[4] For a recent high-yielding synthesis of methanofullerenes, see: Y. Zhang, Y. Matsuo, C.-Z Li, H. Tanaka, E. Nakamura, *J. Am. Chem. Soc.* **2011**, *133*, 8086–8089.

[5] F. G. Brunetti, X. Gong, M. Tong, A. J. Heeger, F. Wudl, *Angew. Chem.* **2010**, *122*, 542–546; *Angew. Chem. Int. Ed.* **2010**, *49*, 532–536.

[6] G. Yu, J. Gao, J. C. Hummelen, F. Wudl, A. J. Heeger, *Science* **1995**, *270*, 1789–1791.

[7] H.-Y. Chen, J. Hou, S. Zhang, Y. Liang, Y. Guanwen, Y. Yang, L. Yu, Y. Wu, G. Li, *Nature Photonics* **2009**, *3*, 649–653; b) S. H. Park, A. Roy, S. Beaupré, S. Cho, N. Coates, J. S. Moon, D. Moses, M. Leclerc, K. Lee, A. J. Heeger, *Nature Photonics* **2009**, *3*, 297–303.

[8] R. D. Kennedy, A. L. Ayzner, D. D. Wanger, C. T Day, M. Halim, S. I. Khan, S. H. Tolbert, B. J. Schwartz, Y. Rubin, *J. Am. Chem. Soc.* **2008**, *130*, 17290–17292.

[9] C. J. Tassone, A. L. Ayzner, R. D. Kennedy, M. Halim, M. So, Y. Rubin, S. H. Tolbert, B. J. Schwartz, *J. Phys. Chem. C* **2011**, *115*, 22563–22571.

[10] a) M. Sawamura, H. Iikura, T. Ohama, U. E. Hackler, E. Nakamura, *J. Organomet. Chem.* **2000**, *599*, 32–36; b) Y. W. Zhong, Y. Matsuo, E. Nakamura, *Org. Lett.* **2006**, *8*, 1463–1466; c) Y. Matsuo, E. Nakamura, *Chem. Rev.* **2008**, *108*, 3016–3028; d) M. Sawamura, K. Kawai, Y. Matsuo, K. Kanie, T. Kato, E. Nakamura, *Nature* **2002**, *419*, 702–705.

[11] T. Niinomi, Y. Matsuo, M. Hashiguchi, Y. Sato, E. Nakamura, *J. Mater. Chem.* **2009**, *19*, 5804–5811.

[12] M. T. Rispens, A. Meetsma, R. Rittberger, C. J. Brabec, N. S. Sariciftci, J. C. Hummelen, *Chem. Commun.* **2003**, 2116–2118.

[13] M. Pope, C. E. Swenberg, *Electronic Processes in Organic Crystals and Polymers*, Oxford University Press, New York, **1999**.

[14] See the Supporting Information.

[15] Spartan′10, Wavefunction, Inc., Irvine, CA.

[16] Shuttlecock molecules with a silylmethyl addend have a less rigid, but also wider and more cylindrical cavity, see: Y. Matsuo, A. Muramatsu, R. Hamasaki, N. Mizoshita, T. Kato, E. Nakamura, *J. Am. Chem. Soc.* **2004**, *126*, 432–433.

[17] For the first synthesized 6,9,12,15,18-pentaaryl-1-hydro[60]fullerenes, see: A. G. Avent, P. R. Birkett, J. D. Crane, A. D. Darwish, G. J. Langley, H. W. Kroto, R. Taylor, D. R. M. Walton, *J. Chem. Soc., Chem. Commun.* **1994**, 1463–1464.

[18] C. Liu, Y. Li, C. Li, W. Li, C. Zhou, H. Liu, Z. Bo, Y. Li, *J. Phys. Chem. C* **2009**, *113*, 21970–21975.

[19] a) V. V. Bashilov, F. M. Dolgushin, B. L. Tumanskii, P. V. Petrovskii, V. I. Sokolov, *Tetrahedron* **2008**, *64*, 11291–11295; b) Y. Matsuo, A. Iwashita, E. Nakamura, *Organometallics* **2008**, *27*, 4611–4617.

[20] Stacking has also been observed recently in a pentaadduct of 9-aza-$(C_{60}\text{-}I_h)[5,6]$fullerene, namely, $6,9,12,15,18\text{-}C_{59}N(CF_3)_5$, see: N. B. Shustova, I. V. Kuvychko, A. A. Popov, M. von Delius, L. Dunsch, O. P. Anderson, A. Hirsch, S. H. Strauss, O. V. Boltalina, *Angew. Chem.* **2011**, *123*, 5651–5654; *Angew. Chem. Int. Ed.* **2011**, *50*, 5537–5540.

[21] H. C. S. Chan, J. Kendrick, F. J. J. Leusen, *Angew. Chem.* **2011**, *123*, 3035–3037; *Angew. Chem. Int. Ed.* **2011**, *50*, 2979–2981.

[22] The crystal structures of $1a\cdot(n\text{-}C_5H_{12})_3$, $1m\cdot CHCl_3$, $1m\cdot CS_2$, $1m\cdot PhMe$, $1m\cdot ODCB$, and $1m\cdot(PhCl)_2$ and their associated CIF files are available from reference [8].

[23] Fullerene centroids were calculated by using the sixty cage carbon atoms.

[24] Molecular formulae in this study represent the theoretical ratios of solvent to pentaarylfullerene present in the crystals if all the solvent regions were fully occupied.

[25] Although most structures could be refined within acceptable parameters, in several cases the solvent regions were partially occupied or contained highly disordered molecules, which often necessitated several squeezes in the crystallographic refinement. CCDC-874453 (**1a** [squeeze]), CCDC-874454 ($1a\cdot(PhCl)_3$), CCDC-874455 ($1b\cdot(n\text{-}C_6H_{14})_{0.5}(ODCB)_{0.5}$), CCDC-874456 ($1b\cdot CS_2$), CCDC-874457 ($1b\cdot NpCl$), CCDC-874458 ($1b\cdot PhCl$), CCDC-874459 ($1c\cdot(CS_2)_{0.5}$), CCDC-874460 (**1d**·[squeeze]), CCDC-874461 ($1d\cdot(PhMe)_{2.7}$), CCDC-874462 ($1e\cdot(PhMe)_3$), CCDC-874463 ($1f\cdot(CHCl_3)_{2.5}(Et_2O)_{0.5}$), CCDC-874464 ($1f\cdot(PhCl)_{1.95}$), CCDC-874465 ($1g\cdot(CS_2)_3$), CCDC-874466 ($1g\cdot(1\text{-}NpCl)_2$), CCDC-874467 ($1g\cdot PhOMe$), CCDC-874468 ($1h\cdot ODCB$), CCDC-874469 (**1i**), CCDC-874470 ($1j\cdot(CS_2)_{0.95}$), CCDC-874471 ($1j\cdot PhMe$), CCDC-874472 ($1k\cdot CH_2I_2$), CCDC-874473 ($1k\cdot(CS_2)_{2.1}$), CCDC-874474 ($1k\cdot ODCB$), CCDC-874475 ($1l\cdot C_6H_{12}$), CCDC-874476 ($1n\cdot(2\text{-}BrC_4H_3S)$), CCDC-874477 ($1n\cdot C_6H_{12}$), CCDC-874478 ($1n\cdot(PhI)_{0.5}$), and CCDC-874479 ($1o\cdot(C_5H_{12})_{0.85}(CS_2)_{0.65}$) contain the supplementary crystallographic data for this paper. These data can be obtained free of charge from The Cambridge Crystallographic Data Centre via www.ccdc.cam.ac.uk/data_request/cif.

[26] A. L. Spek, *Acta Crystallogr. Sect. D* **2009**, *65*, 148–155.

[27] M. W. Bouwkamp, A. Meetsma, *Inorg. Chem.* **2009**, *48*, 8–9.

[28] Y. W. Zhong, Y. Matsuo, E. Nakamura, *J. Am. Chem. Soc.* **2007**, *129*, 3052–3053.

[29] The single crystal diffraction data for the ODCB/*n*-pentane solvate of 4-tolyl derivative **1d** were of low quality. However, the overall packing structure and the unit cell parameters were essentially identical to those of $1d\cdot(PhMe)_3$.

[30] a) L. Sánchez, R. Otero, J. M. Gallego, R. Miranda, N. Martin, *Chem. Rev.* **2009**, *109*, 2081–2091; b) S. Lei, M. Surin, K. Tahara, J. Adisoejoso, R. Lazzaroni, Y. Tobe, S. De Feyter, *Nano Lett.* **2008**, *8*, 2541–2546; c) L. Piot, F. Silly, L. Tortech, Y. Nicolas, P. Blanchard, J. Roncali, D. Fichou, *J. Am. Chem. Soc.* **2009**, *131*, 12864–12865; d) H. L. Zhang, W. Chen, H. Huang, L. Chen, A. T. S. Wee, *J. Am. Chem. Soc.* **2008**, *130*, 2720–2721.

[31] S. Clavaguera, S. I. Khan, Y. Rubin, *Org. Lett.* **2009**, *11*, 1389–1391.